ARC IN AMPA RECEPTOR ENDOCYTOSIS: DIRECT EVIDENCE INDICATING ARC AS A SCAFFOLDING PROTEIN

A THESIS SUBMITTED TO THE GRADUATE DIVISION OF THE UNIVERSITY OF HAWAIʻI AT MĀNOA IN PARTIAL FULFILLMENT OF THE REQUIREMENTS FOR THE DEGREE OF

MASTER OF SCIENCE

IN

CELL AND MOLECULAR BIOLOGY

MAY 2017

By

Brandee M.S.S. Goo

Thesis Committee:

Nicholas G. James, Chairperson
David M. Jameson
Mariana Gerschenson

ACKNOWLEDGMENTS

I would like to thank my advisor, Dr. Nicholas G. James, for his patience, guidance, and support throughout this project. Thank you for taking the time to teach me the biochemistry and fluorescence imaging techniques. I would also like to acknowledge my committee members Dr. David Jameson and Dr. Mariana Gerschenson for their suggestions and expertise. Thank you to Dr. Joseph Albanesi and Dr. Barabara Barylko for providing plasmids and guidance on this project. To Bethany Sanstrum and all of the members of the lab I would like to thank you for helping me through the late nights of columns and imaging.

ABSTRACT

Long-term potentiation (LTP) and long-term depression (LTD) are processes thought to underlie learning and memory, which require proper regulation of activity-regulated cytoskeleton-associated protein (Arc; also known as Arg3.1). Abnormal expression levels of Arc have been associated with Alzheimer's disease, schizophrenia, Fragile-X syndrome, Angelmann's syndrome and substance abuse. Arc is an immediate early gene product that is transcribed in dendritic spines and is a positive regulator of AMPA receptor (AMPAR) endocytosis during LTD. Verified protein-protein interactions between Arc and proteins involved in endocytosis, including dynamin and endophilin, support the role of Arc as a regulator of AMPAR endocytosis. Nevertheless, the mechanism by which Arc specifically targets AMPARs for endocytosis is currently unknown. This is key to understanding the mechanisms of learning and memory and how they are affected by Arc associated human conditions. Here we show evidence of a novel interaction between Arc and protein interacting with C kinase 1 (PICK1), a protein known to bind to the GluR2 subunit of AMPARs and associated with AMPAR trafficking. Cross-correlation raster image correlation spectroscopy and Förster resonance energy transfer (FRET) with Arc-mCherry and EGFP-PICK1 demonstrate this interaction. FRET is more apparent in the projections of transfected SH-SY5Y cells and is enhanced by depolarization. Interestingly, TIRF imaging shows PICK1 aggregates that are only present when cotransfected with Arc that colocalize with Arc aggregates. These findings show an interaction of Arc and PICK1, which may answer how Arc directs endocytic machinery to AMPARs during LTD.

TABLE OF CONTENTS

ACKNOWLEDGMENTS……ii

ABSTRACT……iii

LIST OF TABLES……vi

LIST OF FIGURES……vii

CHAPTER 1. Introduction……1

1.1 Synaptic transmission and AMPA receptors……1

1.2 Mechanisms of long-term depression……2

1.3 Activity-regulated cytoskeleton-associated protein……5

1.4 Protein-interacting with C-terminal kinase 1……6

CHAPTER 2. Materials and Methods……10

2.1 What is fluorescence?……10

2.2 Confocal and total internal reflection fluorescence microscopy……10

2.3 Multiphoton excitation……11

2.4 Fluorescence fluctuation spectroscopy……12

2.5 Raster image correlation spectroscopy……13

2.6 Brightness analysis……15

2.7 Fluorescence lifetime and phasor plots……17

2.8 Förster resonance energy transfer……19

2.9 Materials and methods……21

CHAPTER 3. Results……29

3.1 Arc/PICK1 dynamics in the cytosol……29

3.2 Arc interacts with PICK1……30

3.3 Arc/PICK1 brightness on the plasma membrane……31

CHAPTER 4. Discussion……..……..51

4.1 Role of Arc/PICK1 interaction in learning and memory…….……51

4.2 Future directions…….…….52

REFERENCES……..54

LIST OF TABLES

Table 1. Average fluorescence lifetimes in depolarized and nondepolarized cells……..43

LIST OF FIGURES

Figure 1. General diagram of AMPAR subunit structure……...8

Figure 2. Pull-down of PICK1 from mouse neuronal lysate……..9

Figure 3. Perrin-Jabloński diagram depicting electronic transitions……24

Figure 4. Autocorrelation function determination of diffusion……25

Figure 5. Photon counting histogram……26

Figure 6. Phasor plot…….27

Figure 7. Perrin-Jabloński diagram of energy transfer…….……..……..28

Figure 8. Normalized brightness of Arc-mCherry in the cytosol……...…….…..…33

Figure 9. Concentration dependence of normalized brightness for Arc-mCherry in the cytosol. ……..34

Figure 10. Normalized brightness of EGFP-PICK1 in the cytosol……..35

Figure 11. Concentration dependence of normalized brightness for EGFP-PICK1 in the cytosol……36

Figure 12. Diffusion of Arc-mCherry in the cytosol……37

Figure 13. Concentration dependence of diffusion for mCherry and Arc-mCherry in the cytosol……38

Figure 14. Diffusion of EGFP-PICK1 in the cytosol.……..39

Figure 15. Concentration dependence of diffusion for EGFP and EGFP-PICK1 in the cytosol……40

Figure 16. Diffusion of Arc-mCherry associated with EGFP-PICK1……..41

Figure 17. FRET shows evidence of interaction between Arc and PICK1……..42

Figure 18. Nondepolarized cell with a single lifetime……...…44

Figure 19. Depolarized cell demonstrating energy transfer……...…45

Figure 20. Normalized brightness of Arc-mCherry on the membrane……..…46

Figure 21. Concentration dependence of normalized brightness for Arc-mCherry on the membrane……..47

Figure 22. Normalized median brightness of EGFP-PICK1 on the membrane……...48

Figure 23. Concentration dependence of normalized brightness for EGFP-PICK1 on the membrane……..49

Figure 24. TIRF intensity images of transfected cells…….50

CHAPTER 1. INTRODUCTION

1.1 Synaptic transmission and AMPA receptors

Action potentials carry neural signals from one end of a neuron to the other and are a large component of neural signaling. An action potential is initiated when a neuron receives sufficient depolarizing stimulus to pass a threshold membrane potential. Entry of sodium ions into a postsynaptic neuron is the primary mechanism of membrane depolarization. Glutamate is the primary excitatory neurotransmitter in the brain and may be released from a presynaptic neuron into the synapse in response to an action potential. When glutamate crosses a synapse it can bind to glutamate sensitive receptors on the postsynaptic neuron. These receptors can fall into two-classes: metabotropic and ionotropic. Metabotropic glutamate receptors (mGluRs) initiate intracellular signaling within the postsynaptic neuron that can lead to long lasting structural and functional changes in the cell. In contrast, ionotropic glutamate receptors, which include α-amino-3-hydroxy-5-methylisoxazolepropionate receptors (AMPARs), N-methyl-D-aspartate receptors (NMDARs), and kainate receptors, are ion channels that open to allow the passage of ions across the plasma membrane in response to glutamate binding. These ions can trigger an action potential in the postsynaptic cell as well as act as second messengers.

When activated, AMPARs rapidly open and allow sodium ions into the cell. They are thereby the primary means by which glutamate induces an action potential in a postsynaptic cell. Typical AMPARs are heterotetramers of combinations of GluR1, GluR2, GluR3, and GluR4 subunits. Each subunit contains 3 membrane-spanning regions, a reentrance loop, an N-terminal domain, a glutamate binding region, and a Flip/Flop region (figure 1)[1]. Alternative splicing of the Flip/Flop region varies regionally throughout development and controls the desensitization of the receptor to glutamate activation[2]. Another structural mechanism that regulates the properties of an AMPAR is the stoichiometric composition of its subunits[3]. Homomeric AMPARs containing GluR1, GluR3, or GluR4 allow the passage of sodium and calcium ions into the cell[4]. However, mRNA editing of a glutamine to an arginine in the reentrance loop of the GluR2 subunit prevents the flow of divalent ions, such as calcium, through receptors containing the GluR2 isoform[1]. Subunit composition also affects the trafficking and protein-protein interactions of AMPARs. GluR1 subunits have a relatively long C-terminal cytoplasmic tail in comparison

to GluR3 type subunits[4]. Alternative splicing of the C-terminal region of GluR2 and GluR4 yields both long and short-tailed variants of these subunits[4].

AMPARs are synthesized in the endoplasmic reticulum and modified in the Golgi before being trafficked to the dendrites[4,5]. Evidence of dendritic AMPAR translation has also been demonstrated[6]. At the dendrites, AMPAR surface expression is highly regulated. AMPARs are thought to be inserted into extrasynaptic regions where they diffuse more quickly than those held in the synaptic region[7,8]. Neural activity has been observed to decrease the diffusion rate of AMPARs indicating that AMPAR movement is activity-dependent[7]. In particular, GluR2 containing AMPARs have been indicated to be more synaptically localized following synaptic activity and NMDAR activation[9,10]. Alternatively, GluR1 containing subunits are continually added to and removed from synapses[9,10]. Regulation of surface AMPAR expression is partially controlled by endocytosis and exocytosis. For example, intracellular tetanus toxin, an inhibitor of SNARE-dependent exocytosis, has been shown to decrease AMPAR insertion into the plasma membrane[11]. This implies that AMPARs are likely carried to and from the plasma membrane on vesicles. Centrifugation has been used to identify a fraction of vesicles that contain AMPARs and do not contain NMDARs[12]. These AMPARs were found in intermediate sized vesicles that are in between the size of synaptosomes and synaptic vesicles[12]. In addition, these vesicles were shown to cofractionate with proteins that are known to associate with AMPARs, such as protein interacting with C kinase 1 (PICK1) and GRIP[12]. There are still many questions about the mechanism of AMPAR surface expression regulation and the proteins involved that are under investigation.

1.2 Mechanisms of long-term depression

Understanding the trafficking of AMPARs from the plasma membrane is essential to understanding many diseases and neurological conditions due to the role of AMPARs in learning and memory. Long-term potentiation (LTP) and long-term depression (LTD) are synaptic responses to neural stimulation that are widely thought to underlie learning and memory. LTP is a selective increase in synaptic strength following neural activity that lasts hours or longer. In contrast, LTD is a long-lasting decrease in synaptic response following neural activity. While

the two mechanisms have opposite effects, both processes lead to a change in the excitability of the postsynaptic neuron and are believed to be essential for normal memory formation.

Recently, a causal link between LTP/LTD and memory has been shown using optogenetics to stimulate specific brain regions[13]. Mice were conditionally trained to pair optogenetic stimulation of the amygdala with a foot shock, which was shown to induce LTP at the activated synapse. Following fear conditioning, LTP was reversed using an optogenetic LTD protocol. In this way, researchers were able to erase and reform the foot shock memory using stimulation patterns known to induce LTD or LTP.

In electrophysiology, LTD can be induced through low frequency stimulation or through chemical induction. *In vivo*, LTD is induced through activation of NMDARs or mGluRs. These glutamate receptors initiate signaling cascades via an intracellular flux of calcium ions through NMDARs or by activating G proteins. There are several long-lasting postsynaptic molecular and structural changes that are associated with LTD, which are primarily initiated by these signaling cascades. NMDARs are glutamate receptors that are unique due to their ability to act as coincident detectors[14]. These receptors require both ligand activation by glutamate and depolarization of the postsynaptic membrane to be activated. At rest, the ion channel of NMDARs is blocked by a magnesium ion. When the postsynaptic membrane is depolarized the magnesium ion will leave the pore and allow sodium and calcium ions to flow through the channel. NMDARs are much more permeable to calcium compared to AMPARs, and thereby activate intracellular signaling pathways. This unique mechanism allows NMDARs to open only under conditions in which there is ample signal to depolarize the postsynaptic membrane while the receptor is glutamate bound, resulting in intracellular calcium signaling at these synapses. mGluRs are G protein-couple receptors that are sensitive to glutamate[15,16]. mGluR-dependent LTD is thus due to activation of typical G protein signaling pathways, which can cause long-lasting changes to synaptic transmission.

One type of postsynaptic response associated with LTD is a structural change in spine and dendrite morphology. LTD induction by low frequency stimulation in live mice shows decreased dendritic length, decreased dendritic complexity, and decreased spine density using a Golgi-cox stain in cortical layers[17]. A more detailed view of spine atrophy has been observed using time-lapsed 2-photon confocal microscopy[18]. In this study, the decrease in spine length

was associated with cofilin activity. This is one of several mechanisms associated with LTD that reverses effects observed under LTP-inducing conditions. Rather than a decrease in spine length, LTP is associated by growth of filamentous actin and the formation of new spines[19].

The most commonly studied mechanism of LTD is a decrease in surface expression of AMPARs, as controlled changes in AMPARs provides a clear mechanism for altering efficacy of synaptic transmission. AMPAR concentration at synapses decreases in response to low frequency stimulation and glutamate induction of LTD[20]. Though some AMPARs are constitutively trafficked to and from the membrane, the rate of AMPAR clathrin-dependent endocytosis is increased during LTD[19,21]. LTD-associated decreases in AMPAR membrane localization occurs first in extrasynaptic regions, followed by a decrease at the synapse[22]. This supports the idea that there is lateral diffusion of receptors in the membrane, which can be stabilized at synapses. Instead of endocytosis occurring directly at the synapse, it is believed that changes in extrasynaptic AMPAR concentration indirectly affect the concentration at the synapse.

The protein-dense region at the synapse, which can be seen using electron microscopy, is termed the postsynaptic density (PSD). Proteins in this region, along with actin filaments, control the localization and diffusion of receptors in the PSD. PSD-95/DIgA/ZO-1 (PDZ) domain proteins are highly prevalent in this region as PDZ domains regulate protein-protein interactions as well as association to actin cytoskeleton[10,23,24]. The most well-known PDZ protein is PSD-95, which through its three PDZ domains, directly interact with NMDARs[24]. There are several AMPAR associated PDZ proteins including stargazin, glutamate receptor interacting protein/AMPAR binding protein (GRIP/ABP), and PICK1. These proteins are known to be involved in LTD based on overexpression and knockdown studies, however the precise mechanism of their action has not been determined. The increase in calcium ion concentration and the activation of G proteins due to NMDAR and mGluR activation leads to signaling cascades that may regulate the interactions of PDZ proteins at synapses. Activity of calcium/calmodulin-dependent protein kinase II and protein phosphatase I have been well studied in the regulation glutamate receptors and synaptic plasticity[21,25]. Kinase and phosphatase activity is believed to be critical for the regulation of LTP and LTD due to their ability to alter

protein-protein interactions. Overall, glutamate receptor trafficking and regulation is a process that is highly controlled by many proteins.

1.3 Activity-regulated cytoskeleton-associated protein

It is well known that protein translation is required for both LTP and LTD. Application of protein translation inhibitors, such as cycloheximide, block these synaptic alterations[26]. LTD is unique in that it is not blocked by transcription inhibitors[21]. This implies that LTD relies on pre-transcribed mRNAs. There are several immediate early genes (IEGs) that are rapidly expressed in response to synaptic stimulation and are associated with learning and memory. Activity-regulated cytoskeleton-associated protein (Arc, also known as Arg3.1) is one such IEG that is primarily expressed in the brain[27]. Spatial learning and memory tasks in Arc knockout mice show that Arc is required for long-term memory formation, while short-term memory tasks are not significantly impaired in knockout mice[28]. Wild type aging mice with memory deficits have higher resting levels of Arc translation and lower levels of Arc degradation compared to aged-matched control mice, which may indicate a role of Arc in age-related neurocognitive decline[29]. In humans, altered levels of Arc expression have been associated with Alzheimer's disease[30], schizophrenia[31,32], Fragile-X syndrome[33], Angelman's syndrome[34] and substance abuse[35]. Therefore, understanding the factors involved in Arc expression and its role in synaptic plasticity is important to understanding the mechanisms of these diseases.

Gene expression and localization of Arc are tightly regulated processes that are controlled by neural activity. Electrically induced seizures result in elevated *Arc* mRNA levels in mouse hippocampus within 30 minutes of stimulation[27]. This increase was blocked by NMDAR inhibition. Furthermore, introduction of mice to a novel environment increases dendritic *Arc* mRNA levels in select neurons[36]. The newly transcribed *Arc* mRNA is trafficked to the regions of the dendrite that were stimulated[37–40]. Arc expression levels are also translationally regulated. Glutamate stimulation of neurons expressing recombinant Arc indicate that new Arc is translated within 15 seconds of stimulation in dendrites, which indicates that *Arc* mRNA is likely primed on ribosomes near dendritic spines[41]. The strict regulation of Arc expression and localization to regions of synaptic activity allow Arc to quickly alter synaptic transmission.

A primary role of Arc in AMPAR endocytosis is demonstrated by a decrease in AMPAR surface expression in neurons with overexpressed Arc[42]. This is further supported by an increase in AMPARs in the plasma membrane of Arc knockout[42] and RNAi-mediated Arc downregulation[43] mouse models. Arc is thought to accomplish this task by forming a complex with endocytic machinery, such as endophilin and dynamin[44]. Endophilin is a Bin-Amphiphysin-Rvs (BAR) domain protein that increases synaptic vesicle endocytosis by promoting membrane curvature. Co-immunoprecipitation (co-IP) from cotransfected cells has demonstrated an interaction of Arc with endophilin isoforms 2 and 3 but not 1, which is primarily expressed in the forebrain[44]. Dynamin polymerizes around the necks of budding vesicles and, through GTPase activity, pinches the vesicle away from the membrane. Co-IP has been used to demonstrate an interaction between Arc and dynamin at the PH domain[44]. *In vitro*, Arc facilitates polymerization and enhances GTPase activity of dynamin 2 and 3, which is required for the pinchase activity of dynamin[45]. This effect is not seen with the dynamin 1 isoform, which is primarily expressed in the presynaptic region. Together, these studies demonstrate a role of Arc in postsynaptic vesicle endocytosis whereby Arc facilitates endophilin curvature of the plasma membrane as well as polymerization and GTPase activity of dynamin.

Arc expression is required for proper LTP, LTD, and homeostatic scaling. Electrophysiology studies of Arc knockout mouse hippocampal slices show impaired LTP and LTD[28]. Interestingly, Arc overexpression does not increase endocytosis of all glutamate receptors but is specific to AMPARs[42]. A molecular connection between Arc and AMPARs that explains this specificity has yet to be demonstrated. One group has shown evidence of Arc interaction with TARPγ2 (Stargazin) through 3-dimensional molecular modeling and co-IP[46]. However, this interaction was only demonstrated with a fragmented version of Arc. Preliminary data from a collaboration with Joseph Albanesi (UTSW) showed evidence that Arc interacts with PICK1, a known AMPAR binding protein. GST-Arc was expressed in *E. coli* and purified using glutathione agarose resin followed by Q sepharose chromatography. When incubated with mouse neuronal lysates, PICK1 was found to pull-down with GST-Arc (figure 2). Here we provide evidence of Arc interaction with PICK1, which is a known binding partner of AMPARs. This interaction could explain how Arc specifically facilitates AMPAR endocytosis in mechanisms of learning and memory.

1.4 Protein interacting with C kinase 1

PICK1 is the only known protein that contains both a BAR domain and a single PDZ domain[47]. It also contains an N-terminal acidic domain and a C-terminal acidic domain which regulate the interaction of PICK1 with other proteins[47]. It functions as a scaffolding protein that is widely expressed throughout the body but is primarily enriched in the brain and testis[47]. Over 40 proteins are known to interact with PICK1[48]. Recently, X-ray scattering has been used to show that PICK1 forms dimeric and higher-order self-assembly structures in solution through BAR-BAR association[49]. The PDZ domain is attached to the BAR domain by a long linker region that allows the PDZ domain to be flexible with respect to the BAR domain[48,49].

PICK1 has been shown to interact with the intracellular C-terminal domain of GluR2 and GluR3 AMPAR subunits[50–52]. Studies indicate that this interaction is required for LTD as inhibition of this interaction blocks LTD[11,53]. The PICK1/AMPAR interaction occurs between the PDZ domain of PICK1[53] and 10-C-terminal amino acids of short form alternatively spliced AMPAR subunits[51]. This C-terminal tail is a conserved region that is known as the PDZ binding motif and also interacts with GRIP/ABP[53]. This motif is phosphorylated at S880 by protein kinase C (PKC), which decreases GRIP/ABP association but does not affect PICK1 binding[54]. Thereby a proposed model exists in which GluR2 is bound to GRIP/ABP at rest and is not phosphorylated[53]. Upon glutamate excitation of the postsynaptic neuron, PKC is activated by NMDARs or mGluRs. PKC can be activated by calcium ions which enter the cell upon NMDAR activation[55]. Alternatively, PKC can be activated by diacylglycerol and calcium ions through mGluRs that activate phospholipase C through a G protein associated pathway[55]. PKC then phosphorylates the intracellular C-terminal tails of GluR2 to facilitate the release of GRIP/ABP and binding of PICK1 to the tail[53]. This process is further enhanced by the binding of calcium ions to the N-terminal acidic tail of PICK1, which increases the affinity of PICK1 for GluR2[56–58].

Here we show evidence of Arc/PICK1 interaction in live human neuroblastoma cells using fluorescently tagged Arc and PICK1. This interaction fills a hole in the current model of AMPAR internalization during LTD. When PICK1 binds to AMPARs, Arc association with endocytic machinery could explain how AMPARs are selectively internalized.

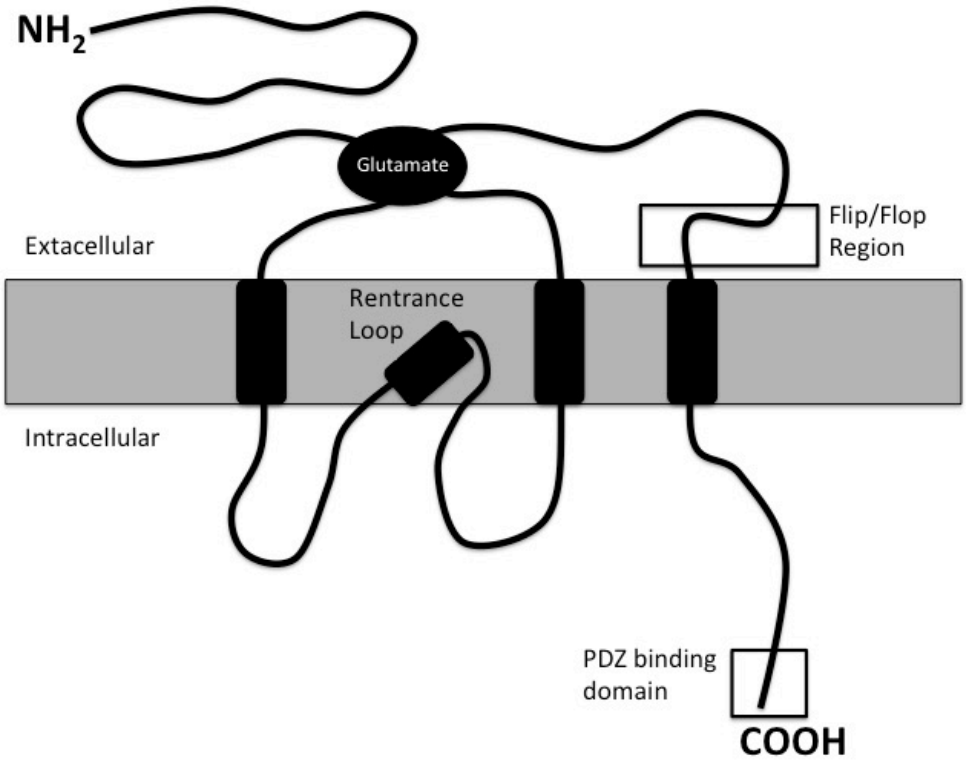

Figure 1. General diagram of AMPAR subunit structure

All subunits contain three membrane-spanning domains, a reentrance loop, an extracellular N-terminal, an intracellular C terminal, and a glutamate binding region. The flip/flop region and the length of the C terminal tail vary between subunits due to alternative splicing.

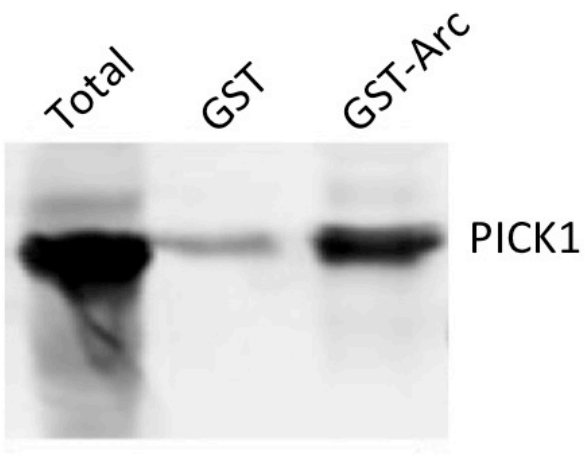

Figure 2. Pull-down of PICK1 from mouse neuronal lysate

Purified GST-Arc was incubated with mouse neuronal lysate and pulled down using glutathione agarose. Western blot using PICK1 specific antibody demonstrates that PICK1 can be coprecipitated with Arc.

CHAPTER 2. MATERIALS AND METHODS

2.1 What is fluorescence?

Certain atomic elements and molecules are capable of absorbing electromagnetic energy to transition to an excited electronic level[59]. Some molecules can release this excited state energy in the form of fluorescence upon transitioning to the ground state. The observation of fluorescence has come a long way since it was first described in 1565 by Nicolas Monardes when he observed a bluish emission after *Lignum nephriticum* was placed in water and excited by sunlight[59,60]. The compound from this wood that is responsible for the observed fluorescence has a four ring structure[60]. The conjugated ring in this structure, as with most fluorescent compounds, decreased the energy required to excite the π electron to the π^* orbital[59,60]. According to the Franck-Condon principle, this change in electronic state occurs very fast in comparison to changes in bond configuration, therefore the molecule retains its original bonding[59]. As shown in the Perrin-Jabloński diagram of electronic energy (figure 3), vibrational relaxation and internal conversion occurs when an electron is excited above the lowest vibrational level, S_1[59,60]. Therefore, photon emission (fluorescence) almost always occurs during the S_1 to S_0 relaxation and is not affected by the excitation wavelength[59,60]. Absorption, vibrational relaxation, and internal conversion all occur quickly, on the order of 10^{-12} seconds or shorter[59]. However, interactions with the solvent or matrix and the structural arrangements of fluorophores will have a significant effect on how long the electron will remain in the S_1 state before returning to the ground state, termed the fluorescence lifetime. Lifetime is an intrinsic property of a particular fluorophore and is on the timescale of picoseconds to nanoseconds. Our understanding of fluorescence has greatly improved in the past few centuries and the development of new technologies has allowed us to utilize fluorescence in the study of biological processes down to the nanometer scale.

2.2 Confocal and total internal reflection fluorescence microscopy

There are a large number of methods one can use to record fluorescence emission. Traditionally, fluorescence parameters, such as steady-state emission, polarization, and lifetime of pure fluorescent molecules are recorded in a Quartz cuvette using a fluorimeter[59]. These methods gather measurements from a solution of several hundred microliters to several milliliters

and therefore yield an average of the sample. To examine the inner working of proteins in live cells using fluorescence one must generate detection volumes in the submicrometer range. Laser microscopy has emerged as a powerful method to generate small volumes to investigate protein dynamics in cells. Confocal and total internal reflection fluorescence (TIRF) microscopy are complimentary methods that allow for selected excitation of the cell interior or one surface of the plasma membrane, respectively.

The confocal microscope was first invented in 1955 by Marvin Minsky with the hope of more clearly imaging neural networks by decreasing the effect of out of focus light[61,62]. Images from an epifluorescence microscope are blurred, making fine structures difficult to resolve. Minsky's original design used two separate objectives for excitation and emission and the light source and detection was limited by the use of pinholes[61]. This greatly decreases the excitation and detection volume to a focused spot rather than an entire cell. Therefore Minsky designed a moving stage so that the cell is moved over the excitation volume. A complete image is then pieced back together through computer software. Today, most confocal microscopes are laser scanning so that the excitation beam is moved over the sample rather than moving the stage. This provides a more precise method that is less sensitive to vibration.

While confocal microscopy is the superior method to image the cytosol of a cell with high resolution, TIRF microscopy is a specialized technique to study the dynamics near the plasma membrane. This is accomplished by aiming the excitation laser with a high incident angle on the coverslip[63–66]. When the laser reaches the cell (low refractive index), the laser will be reflected back through the glass coverslip (high refractive index). An evanescent wave of light will penetrate the sample within less than 100 nanometers above the coverslip. Therefore in cells only the molecules near or in the plasma membrane closest to the laser will be excited.

2.3 Multiphoton excitation

Multiphoton excitation was first described in 1931 by Maria Göppert-Mayer in her doctoral thesis[59,67]. This method requires two or more photons, at approximately twice the wavelength (half the energy) required for one-photon excitation, to be nearly simultaneously absorbed by the fluorophore to bring about an electronic transition (figure 3). Exciting the sample in this manner has several benefits over the relatively inexpensive one-photon confocal microscopy. This

method is inherently confocal without the use of pinholes as the concentration of photons to adequately excite the sample is high enough only at the focal point. As the distance from the focal point increases, the intensity is decreased by the distance squared[68]. Therefore, out of focus light is also eliminated yielding a much clearer image[59,69]. Live cell imaging always comes with the risk of generating light-induced reactive oxygen species and photobleaching[70]. Both processes can affect the quality of the images collected, however they are reduced when using multiphoton excitation. In addition, the high wavelength used reduces light-scattering and allows the beam to penetrate thick samples[69].

Two-Photon confocal microscopy requires a high concentration of photons at the focal point at the same time to increase the probability that two photons will be absorbed. Typical systems accomplish this with a titanium:sapphire laser which has the ability to produce pulsed light with high power in the 700 – 1000 nm range[59,69]. Overall, the pulsed nature of the excitation yields a low average power to the sample. The development of instrumentation that is able to excite and detect fluorescence has enabled the development of new techniques to quantify its properties.

2.4 Fluorescence fluctuation spectroscopy

As fluorophores move into and out of the excitation volume of a microscope, the detected intensity signal will fluctuate (figure 4A). In a steady-state system, such as a fluorimeter, the excitation volume is too large to observe these fluctuations. However, confocal and TIRF optical arrangements are able to record these events. These fluctuations, particularly when collected with a low fluorophore concentration, can be quantified to reveal useful information about the sample. Fluorescence correlation spectroscopy (FCS) uses the temporal aspect of the fluctuation signal to calculate the concentration and diffusion values. The rate of diffusion of the fluorescent compound can be extracted using an autocorrelation function given by

$$G(\tau) = \frac{<\delta F(t)\delta F(t+\tau)>}{<F(t)>^2} \qquad (2.1)$$

where $G(\tau)$ is the autocorrelation function, $<F(t)>$ is the average intensity, and $\delta F(t)$ is the difference from the average intensity ($\delta F(t) = F(t) - <F(t)>$)[59,71]. This is calculated over the data

set to yield an autocorrelation function (figure 4B). In this function, the fluorescence intensity signal is correlated with itself at a later time point, τ. Therefore correlation is higher at lower values of τ and the signals become less correlated as τ increases. This gives the autocorrelation function the distinctive shape seen in figure 4B. Logically, slower diffusing fluorescent compounds will remain correlated over a larger range of τ values due to the persistence of the molecule within the excitation volume. In this instance, a shift of the autocorrelation function to the right can be observed (figure 4B). Therefore, the rate of diffusion can be acquired from the autocorrelation function, given knowledge of the excitation volume (commonly called the point spread function). When applied to a biological system, a change in the rate of diffusion of a fluorophore can be used to detect an interaction between the fluorophore, or fluorescently tagged molecule, and another molecule or biological structure.

In the autocorrelation function when τ is equal to zero the equation can be reduced to the square of deviation from the average over the average squared for the data set. This value is proportional to the number of molecules in the detection (N) volume following equation 2.2[71].

$$G(0) = \frac{1}{N} \qquad (2.2)$$

By knowing the detection volume, the concentration of fluorophores in the sample can be determined. This can be applied to samples in solution as well as to live cells. Methods in fluorescence fluctuation spectroscopy (FFS), and which use fluctuations in an intensity signal to characterize the dynamics of fluorophores, have advanced with the advent of new instrumentation to collect data and software for analysis.

2.5 Raster image correlation spectroscopy

FCS is a single point method and can only determine the rate of diffusion of fluorescent molecules at one point. Therefore, one would need to collect data at several points to determine how fluorescent molecules move within different areas under non-homogeneous settings, such as the interior of a cell. A number of methods have been developed to provide spatial information of molecule diffusion within a cell[72]. The raster image correlation spectroscopy (RICS) method was developed to isolate diffusion and sample concentration over an image rather than at a single

point, allowing more spatial information to be gathered from a system such as live cells[73]. RICS was first developed and described by Enrico Gratton's laboratory (Laboratory for Fluorescence Dynamics, UCI) in 2005[74]. RICS analysis is applied to a raster scanned image collected using a laser scanning microscope. In this type of scanning, the top row is collected left to right. The laser then retraces to the left and collects the second row. Once the full region of interest is collected, the laser will return to the top left corner to collect a new frame. RICS takes advantage of the inherent time and position properties of an image collected in this manner. Depending on the pixel dwell time, the pixel to pixel time is on the order of microseconds and the line to line time is on the order of milliseconds. Therefore, RICS can detect fast moving particles as well as slow moving particles. During RICS analysis, the first step is subtraction of the moving average, which will remove the signal that is due to immobile or slow moving fluorophores[73]. By subtracting the moving average, this method can better be applied to cells that frequently move on the cell culture dish. Then correlation functions are applied to each frame as follows

$$G_{RICS}(\xi, \Psi) = \frac{< I(x,y) I(x+\xi, y+\Psi) >}{< I(x,y) >^2} - 1 \qquad (2.3)$$

where I is the intensity at the stated pixel, ξ is the spatial increment in the x direction, Ψ is spatial increment in the y direction, and the brackets represent the average over all pixels in the image[74]. For each frame, the correlation is conducted for each possible pixel and spatial increment. The values from each frame are then compiled and averaged. Multiple frames are used to improve the signal-to-noise ratio and as a reference for the average subtraction[73]. For a non-homogenous sample, such as protein aggregates in cells, RICS can be separately conducted in regions that contain aggregates and regions that do not contain aggregates. In this manner, RICS can be used to more fully understand the dynamics of a complex system.

The correlation method used in RICS has been expanded to cross-correlation RICS (ccRICS) in which the signal in one channel is compared to the signal from a second channel rather than being correlated with itself. By doing so, the simultaneous movement of two different fluorophores that are acquired by separate detectors can be compared according to

$$G_{ccRICS}(\xi, \Psi) = \frac{< I_1(x,y) I_2(x+\xi, y+\Psi) >}{< I_1(x,y) >< I_2(x,y) >} - 1 \qquad (2.4)$$

where I_1 is the intensity collected through the first detector and I_2 is the intensity collected by the second detector[75]. The correlation is then due to fluorescence fluctuation intensity signals that move together in both channels, rather than due to the detection of the same particle at different spatial and temporal locations. If the two fluorescent particles are moving together, this provides strong evidence that the compounds are interacting in some way. ccRICS has obvious applications to biological applications, particularly protein-protein interaction.

2.6 Brightness analysis

One limitation of FCS and RICS analysis is that the raw data is reduced and fluctuations are only examined in the time domain. Diffusion is determined by the size and interaction of the fluorophore with its environment. For a sample in solution, the size of the particle is associated with its diffusion by the Stokes-Einstein-Sutherland equation[72]. Accordingly, a change in oligomerization state from a monomer to a dimer changes the diffusion by only a factor of 1.26[76], which makes detecting changes in fluorophore association by diffusion difficult. Determining the oligomerization state through diffusion measurements is even more difficult in cells as the diffusion of molecules in the complex environment of living cells is greatly decreased[72]. This raises the question of how to quantify monomer/dimer equilibriums. To determine this one turns to examining the intensity fluctuation rather than the time domain. In 1999 two groups independently reported FFS methods extracting molecular brightness and number of molecules as a means to determine the oligomerization state of a fluorescent molecule[71,77,78]. For the purpose of this thesis we will be using the terminology from the Gratton group, i.e. Photon Counting Histogram (PCH). An intensity data stream is collected in a single location for a fixed amount of time with a fixed sampling frequency. Each intensity measurement is plotted into a histogram. The shape of the histogram is fit to a mathematical model based on a number of molecules in the excitation volume (N) and a brightness (B) value in counts per second per molecule (cpsm) (figure 5). Logically, an aggregate will have more

counts per molecule compared to a monomer. As this aggregate moves into or out of the detection volume, a larger intensity fluctuation from the average will occur compared to compared to the movement of a monomer. This will cause the shape of the histogram to widen as the variance in the data set has increased. Therefore a wider histogram is attributed to a higher oligomerization state.

PCH is a statistically rigorous method that requires a long data stream to accurately determine the oligomerization state and number of molecules in the detection volume and is therefore applied to a single detection volume. Typically a 3 – 5 minute fluorescence intensity signal is collected for a single point. This works well for a homogenous solution, however when applied to live cells, it provides very limited information about the complexity of cell that is reduced to one or two brightness values for each cell. Brightness analysis has since been expanded to a set of images through number and brightness (N&B) analysis[79,80]. This method is applied to a set of images of a cell acquired by confocal or TIRF microscopy. The time required for data collection greatly depends on the number of frames collected and the speed at which each image is generated. N&B can be applied to an entire cell because the brightness can be determined directly from the intensity data. The N and B values determined for each pixel of the image are calculated based on the equations derived and published by Enrico Gratton's laboratory (Laboratory for Fluorescence Dynamics, UCI)[79].

$$N = \frac{< k >^2}{\sigma^2} = \frac{\varepsilon n}{\varepsilon + 1} \tag{2.5}$$

$$B = \frac{< k >}{N} = \frac{\sigma^2}{< k >} = \varepsilon + 1 \tag{2.6}$$

where <k> is the average intensity, σ^2 is the variance of the intensity, N is the apparent number of molecules, B is the apparent brightness, n is the number of particles in the detection volume, and ε is the molecular brightness. Using Globals for Images (SimFCS software from the Laboratory for Fluorescence Dynamics) N&B analysis not only allows a simple quantification of the oligomerization state in the cell but provides a pixel-by-pixel spatial distribution of the B

values. The localization of various oligomerization states throughout a cell can be determined to give the user more information about the fluorophore dynamics in the cell. This method can easily be paired with fluorescently tagged proteins in live cells to determine protein dynamics and stoichiometries of protein complexes. This is particularly useful to study proteins that are active as oligomeric compounds.

N&B analysis can be combined with TIRF microscopy to determine protein self-association state at the plasma membrane[81]. The N&B equations have been adjusted for use with analog detection to subtract noise in the signal originating from an electron-multiplied charge-coupled device (EMCCD) camera:

$$N = \frac{(<I> - offset)^2}{\sigma^2 - {\sigma_0}^2} \tag{2.7}$$

$$B = \frac{\sigma^2 - {\sigma_0}^2}{<I> - offset} \tag{2.8}$$

where *offset* is the intensity associated with the camera when the laser is off (dark counts) and σ_0^2 is the variance of this intensity[81].

2.7 Fluorescence lifetime and phasor plots

The fluorescence lifetime is the amount of time that an electron of a fluorophore stays in the excited state, S_1, before returning to the ground state and causing the release of a photon in the form of light. This lifetime can vary from picoseconds to hundreds of nanoseconds depending on the fluorophore. There are two methods commonly used to determine the lifetime of a fluorophore: the time domain and the frequency domain. Typically these methods are used to study a population of molecules rather than a single molecule as the lifetime of a single fluorophore can vary from excitation to excitation but a population of fluorophores will have a characteristic lifetime.

The time domain or impulse response approach uses a short pulse of light, shorter than the lifetime, to excite the sample and records the subsequent intensity[59]. The intensity over time will follow an exponential decay[82]. The lifetime, τ, is the time at which the emission intensity

decreases to 1/e of the maximum emission intensity. Fluorophores can have simple decay kinetics (single exponential decay), however, it is very common for fluorophores to contain complex decay kinetics (multi-exponential decay). These complex decay patterns are often characterized by the sum of the single exponential contributions to the emission.

The second method used to determine lifetime is the frequency domain or harmonic response approach. This technique was first successfully used by Enrique Gaviola in 1926 to determine the lifetime of rhodamine and fluorescein[59,83] and evolved to its modern incarnation by Weber, Spencer, and Gratton[84–86]. Sinusoidally modulated light is used to excite the sample and the resulting fluorescence intensity is measured. The emission intensity has the same frequency but is shifted in time and demodulated (lower intensity)[83]. The equations used to derive the lifetime were first described by F. Dushinsky in 1933[59]:

$$\Phi = \arctan(\omega\tau_P) \tag{2.9}$$

$$M = \frac{\left(\frac{AC}{DC}\right)_{Emission}}{\left(\frac{AC}{DC}\right)_{Excitation}} \tag{2.10}$$

$$M = \frac{1}{\sqrt{1+(\omega\tau_M)^2}} \tag{2.11}$$

where Φ is the phase delay, ω is the angular frequency ($2\pi f$, where f is the linear modulation frequency), AC is the difference between the emission intensity and the average intensity, DC is the average intensity, and M is the relative modulation. A different phase lifetime, τ_P, and modulation lifetime, τ_M, can therefore be calculated for a sample. For a sample with simple decay kinetics the phase lifetime and modulation lifetime will be equal. These measurements may be conducted over multiple frequencies in order to parse out the separate lifetimes that contribute to a sample when the fluorophore shows complex decay kinetics[87]. The phase delay and modulation are plotted against several excitation frequencies. These data are then fit to a model to determine the lifetime components involved.

More recently, the phasor plot method has been used to represent the data and gather information about the lifetimes that contribute to a sample without having to fit the data to a model. Phasor plots are a way to present the data so that it is easier to see the lifetime components and the trajectory of lifetime values in response to changes in sample components. In 1981, Gregorio Weber, who was instrumental in advancing fluorescence methodologies, derived the two equations used in phasor plot analysis[84].

$$S = M\sin\theta \tag{2.12}$$

$$G = M\cos\theta \tag{2.13}$$

The phasor plot is constructed in which the lifetime measurement is depicted as a vector on an x-y axis with G as the x-axis and S as the y-axis (figure 6). Here the angle between the x-axis and the vector is the phase delay and the length of the vector is M[83,88,89]. A semi-circle with a radius of 0.5 with its center at (0.5,0) is designated the universal circle. Lifetime measurements will only fall on the universal circle if they have a single exponential lifetime. Any other lifetime measurements will fall inside the universal circle. In this way, phasor plots represent an easy method to determine if a sample has more than one lifetime component.

2.8 Förster resonance energy transfer

More recently, phasor plots have been applied to the study of fluorescence lifetime imaging microscopy (FLIM) and Förster resonance energy transfer (FRET)[88]. FLIM is fluorescence lifetime applied to an image so that spatial information can be gathered. When converted to a phasor plot, a distribution of pixels on the phasor plot can be visualized with each pixel corresponding to a pixel of the image. Using the Globals for Images software (Laboratory for Fluorescence Dynamics) a cursor may be moved over the phasor plot so that the regions of the image with the corresponding lifetime can be easily visualized. This method is particularly useful in cells so that the spatial location of species with different lifetimes can easily be determined. Also, the raw data is used to produce the phasor plot so it requires significantly less photons to accurately describe the kinetics within the cell.

FRET was named after Theodor Förster who published seminal articles on the topic in 1946[90,91], though energy transfer was originally observed in the 1920s through polarization studies[59]. Since this time, our understanding and use of FRET have greatly advanced. A donor molecule whose fluorescence emission wavelengths overlap with that of the acceptor absorbance is required[87]. If the donor and acceptor are in close enough proximity and their dipoles are appropriately aligned, then the donor can transfer excited energy to an acceptor[59,92]. The energy transfer is a nonradiative process such that a photon is not emitted but rather vibrational energy is transferred from the excited donor to the acceptor molecule, as shown in the Perrin-Jabloński diagram of resonance energy transfer (figure 7). The distance required for energy transfer to occur is typically within 10 – 100 Å, however the exact distance required varies between each donor-acceptor pair[87]. For an EGFP-mCherry donor-acceptor pair, this distance is reported as 52.4 Å[93]. Therefore, observation of FRET provides strong evidence that a protein complex between the acceptor and donor has formed[88]. Due to the distance and orientation required for FRET, however, the absence of energy transfer does not establish that two molecules do not interact.

There are two popular methods used to determine FRET, steady-state intensity and the time-resolved method. Steady-state intensity is based on changes of the fluorescence intensity of the donor molecule. A decrease in intensity would indicate that some of the energy absorbed by the donor is no longer being lost through photon emission in the presence of the acceptor. Though the instrumentation required for this method may be more accessible, and this is the most commonly used method to measure FRET, the emission intensity will be dependent on the concentration of the molecules and the excitation power. The second approach, the time-resolved method, avoids this constraint by relying on fluorescence lifetime measurements. Fluorescence lifetime is an intrinsic property of the fluorophore and will not vary with concentration. When FRET occurs, a decrease in the fluorescence lifetime of the donor will be observed[88]. When measured in cells, the lifetime of the fluorophore will move from the donor lifetime toward a location in the circle that is consistent with the lifetime of cellular autofluorescence. As the efficiency of energy transfer increases, the points will move closer to the autofluorescence lifetime. FRET is a useful approach to determine molecular interactions due to the close proximity required for energy transfer to occur. When combined with methods

such as FLIM and phasor plot representation, FRET can easily be used as evidence of spatial location of interaction in a dynamic cell system.

2.9 Materials and methods

Cell Culture and Transfection

SH-SY5Y cells (ATCC®), bone marrow derived human neuroblastoma cells, were cultured in phenol red-free DMEM F12 (Gibco™) containing 15mM HEPES, 1.5mM sodium pyruvate, 1x Antibiotic-Antimycotic and 20% FBS (ATCC®) in tissue culture-treated T75 flasks (Corning™) at 37°C, 5% CO_2. Cells were lifted with a 0.08% solution of trypsin-ethylenediaminetetracetic acid solution in PBS. Cells were plated onto uncoated 10mm glass bottom dishes (MatTek) and transfected with Lipofectamine™ 3000 (Invitrogen™) following the manufacturer's protocol with 0.2-1.5μg DNA per plasmid per dish. Arc and PICK1 plasmids were kindly provided by Dr. Joseph Albanesi (UTSW). A mouse variant of Arc was ligated to mCherry at the C terminus. A human variant of PICK1 was ligated to EGFP at the N terminus. For depolarization studies, cells were washed in PBS and imaged in either depolarizing buffer (42mM NaCl, 100mM KCl, 0.6mM $MgSO_4 \bullet 7H_2O$, 2.5mM $CaCl_2$, 6mM D-glucose, 10mM HEPES, pH 7.4) or nondepolarizing buffer (135mM NaCl, 5mM KCl, 0.6mM $MgSO_4 \bullet 7H_2O$, 2.5mM $CaCl_2$, 6mM D-glucose, 10mM HEPES, pH 7.4) after 15 minute incubation.

Two-photon confocal imaging

FFS measurements were recorded on an Alba fluorescence correlation spectrometer (ISS, Champaign, IL), equipped with x-y scanning mirror, connected to a Nikon TE2000-U inverted microscope (Nikon, Melville, NY) with a PlanApo VC 60 x 1.2 NA water objective. Two-photon excitation of enhanced green fluorescent protein (EGFP)-PICK1 and mCherry-Arc was provided by a Chameleon Ultra (Coherent, Santa Clara, CA) tuned to 1000 nm. Fluorescence emission was spectrally filtered through a 680 nm short-pass filter (FF01-680; Semrock, Rochester, NY) and dichroic mirror (700dcxru, Chroma, Bellows Falls, VT) with intensity of EGFP and mCherry collected on individual PMTs. Cells were imaged in a humidified enclosed chamber kept at 37ºC (Tokai Hit, Fujinomiya, Sizuoka, Japan). An objective heater wrapped

round the neck of the objective was used to minimize temperature drifts (with a 20 minute delay to equilibrate the temperature prior to imaging) and the collar of the objective was adjusted to compensate for temperature and thickness of the coverslip.

RICS was used to examine the protein dynamics in live cells. Briefly, 12.8 micron (50 nm pixels) regions of interest were selected from the fluorescence image. The pixel sampling time was 12.5 μs, each frame had 256 x 256 pixels, and each measurement lasted ~ 1 min (100 frames). The laser power at the sample was < 1 mW. The beam waist (ω_0) calibration was achieved by measuring the autocorrelation curve of fluorescein (~ 20 nM) in 0.01 M NaOH, and fitted with a diffusion rate of 430 μm^2/sec, which were performed before each day's measurement. The typical values of ω_0 were at the range of 0.35 – 0.4 μm.

For the PCH measurement, the laser excitation point was selected in a region of the cytosol away from the nucleus and plasma membrane. Intensity fluctuations were recorded for ~ 4 minutes with sampling rate of 50,000 Hz. Monomer brightness of EGFP is obtained by averaging cells transfected with monomeric EGFP at various protein concentrations. Brightness values were calculated using Vinci software with incorporation of the dead-time of the detectors (50 ns).

FLIM measurements were recorded through an ISS A320 FastFLIM box coupled to the Ti:Sapphire laser, which produces 80-fs pulses at a repetition rate of 80 MHz, and photo multiplier detector (H7422P-40, Hamamastu, Hamamastu City, Japan). EGFP was excited at 920 nm and the fluorescence signal was filtered away from excitation light through a 520 nm bandpass filter (FF01-520/35; Semrock Rochester, NY) mounted in front of the detector.

TIRF imaging

Images were recorded on a Nikon Eclipse Ti Total Internal Reflection Fluorescence microscope using a 60 x 1.45 NA oil objective. A cascade 512B EMCCD camera (Photometrics, Tucson, Az) equipped with a dual view image splitter was used to image EGFP and mCherry at 100 frames/s. Both proteins were excited simultaneously at 488 nm for EGFP and 543 nm for mCherry using a triple band excitation filter (405/488/594 nm; Chroma, Bellows Falls, VT) within the infinity space.

Data Analysis

PCH was analyzed using VistaVision software (ISS). RICS, N&B, and FRET were analyzed using Globals for Images (SimFCS software from the Laboratory for Fluorescence Dynamics). Comparison between groups was carried out using multivariate ANOVA using Bonferroni post-hoc. Statistical significance was accepted when $p<0.05$. Statistical analyses were performed using SAS University software.

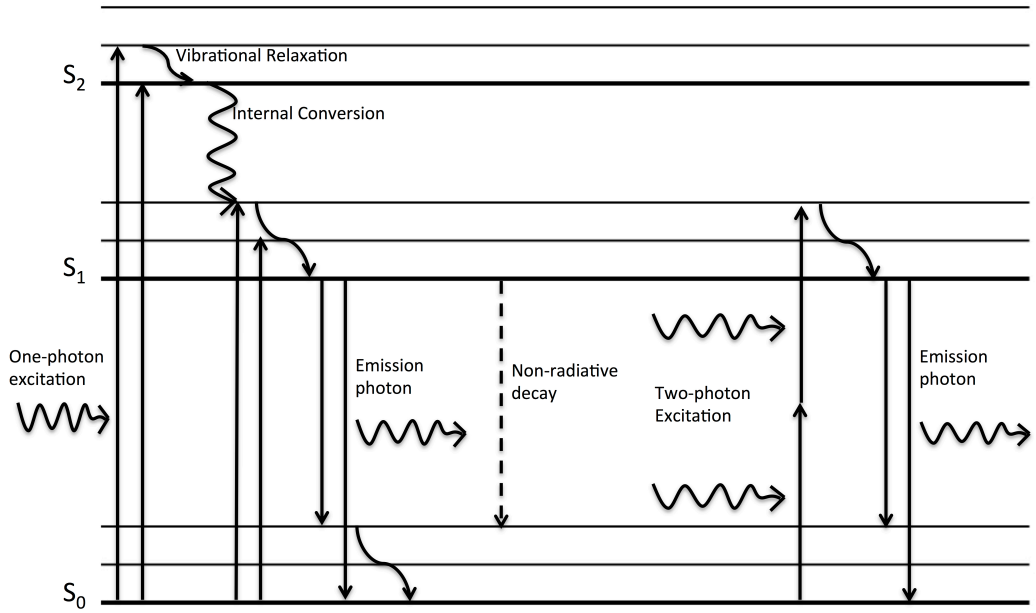

Figure 3. Perrin-Jabloński diagram depicting electronic transitions

For one-photon excitation (left) the absorption of a photon excites an electron from the ground state (S_0) to the excited state (S_1 or S_2). Vibrational relaxation and internal conversion rapidly bring the electron to the S_1 state. The electron then returns to the ground state by non-radiative decay or through the release of a photon (fluorescence). Alternatively two-photon excitation (right) requires two photons of half the energy to excite the electron near simultaneously to bring it to an excited state.

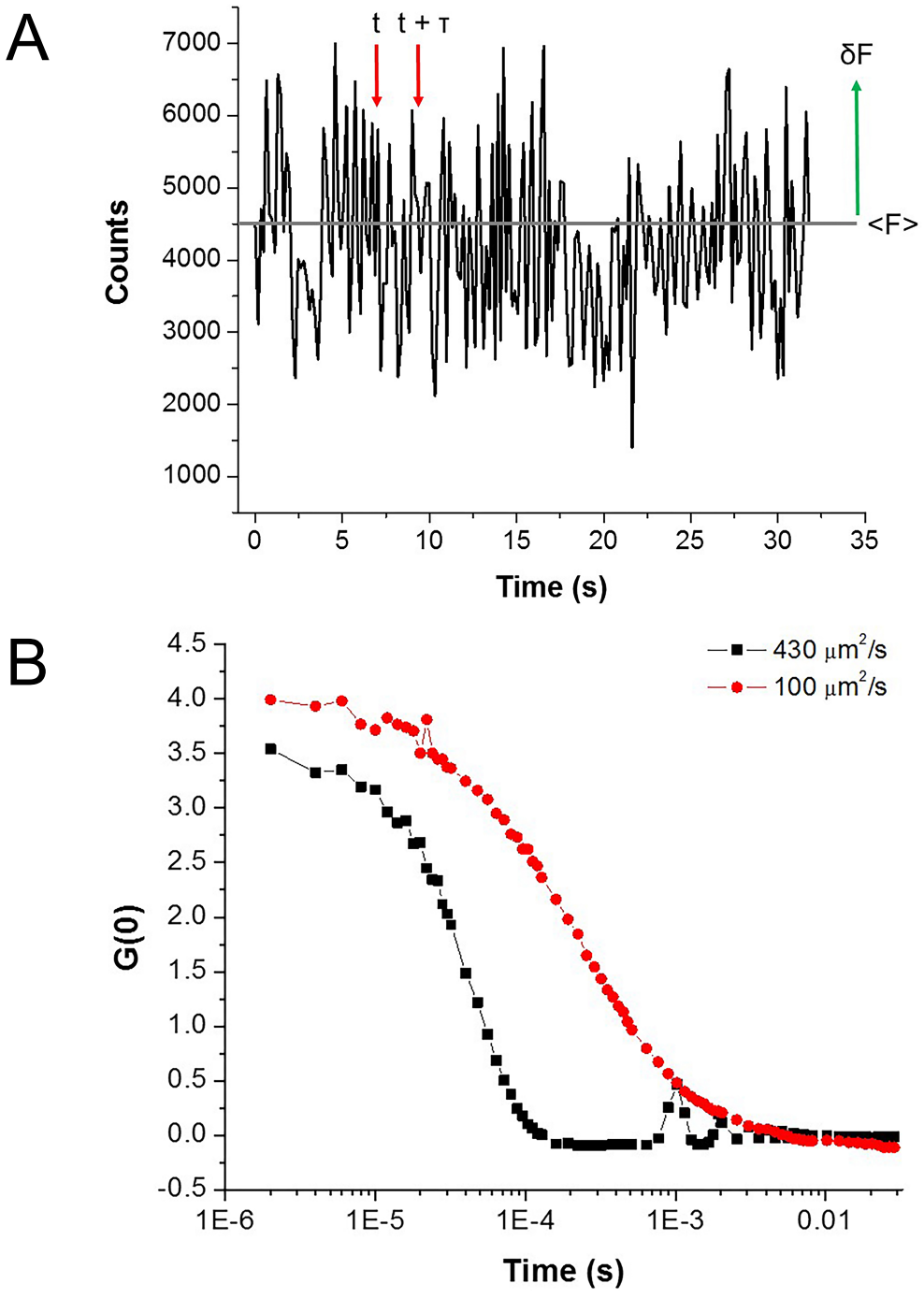

Figure 4. Autocorrelation function determination of diffusion

A. Fluorescence intensity data simulated using SimFCS showing fluorescence fluctuations. B. Autocorrelation function of simulated data with a diffusion rate of 430 $\mu m^2/s$ and 100 $\mu m^2/s$, shows the difference in the autocorrelation function due to the rate of diffusion. At a slower rate of diffusion, the curve shifts to the right.

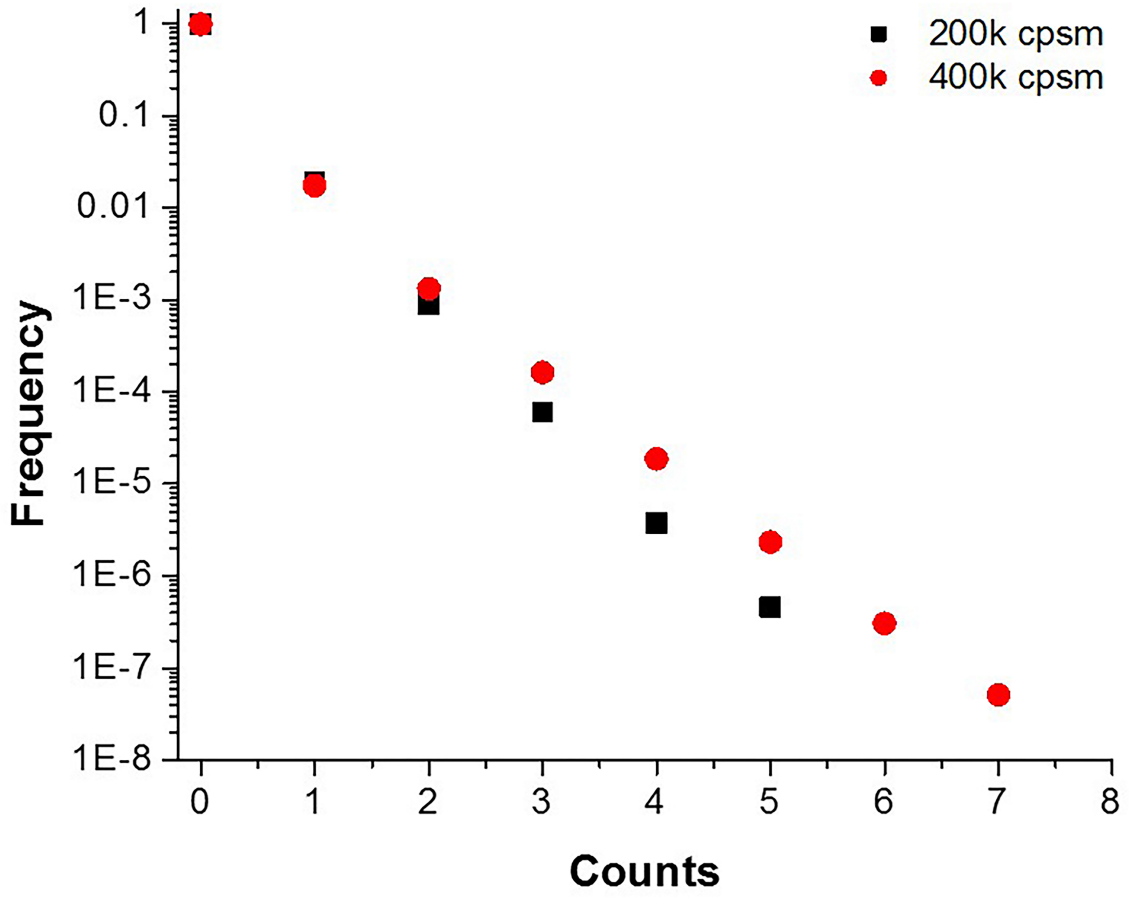

Figure 5. Photon counting histogram

A histogram of data simulated using SimFCS for a sample of molecules with a brightness of 200k cpsm and 400k cpsm. With a higher brightness value, the histogram broadens due to larger fluctuations in the data stream.

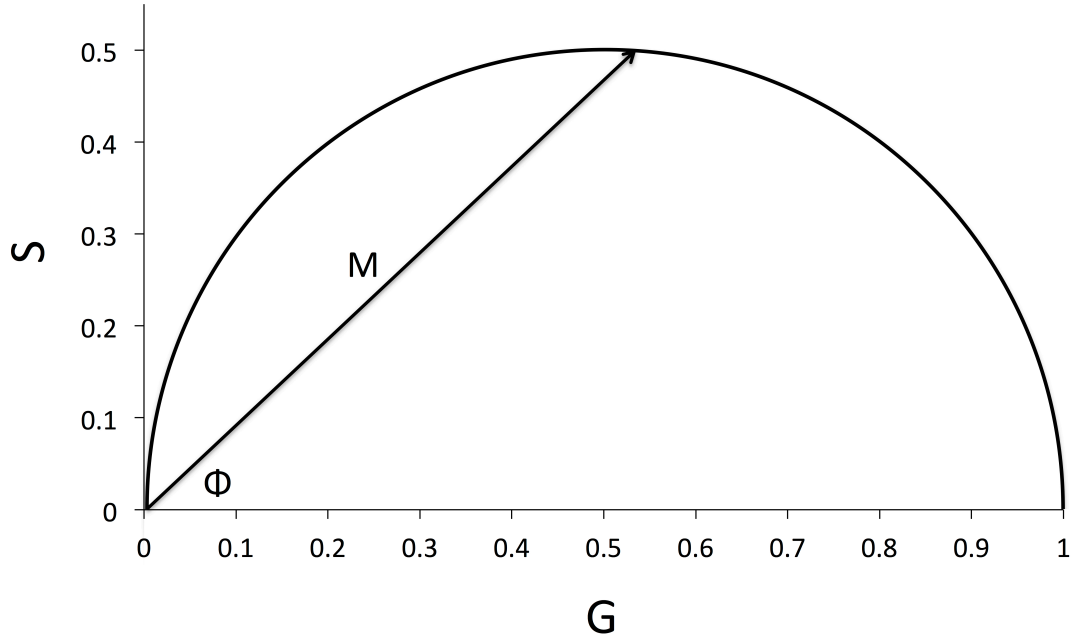

Figure 6. Phasor plot

Phasor plot depicting the universal circle and a vector representing a single-exponential lifetime.

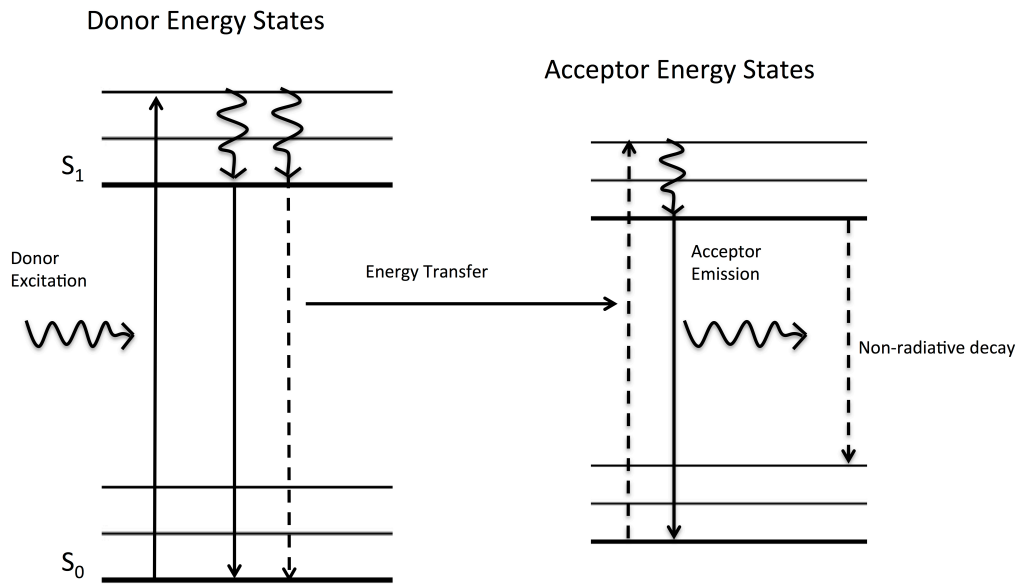

Figure 7. Perrin-Jabloński diagram of energy transfer

Energy transfer can occur from an excited donor to an acceptor molecule. If the acceptor is a fluorophore, it can fluoresce when returning to the ground state. Otherwise the excited electron will return to the ground state by non-radiative means.

CHAPTER 3. Results

3.1 Arc/PICK1 dynamics in the cytosol

In order to characterize the dynamics of Arc and PICK1 in live cells, we transfected SH-SY5Y cells with recombinant Arc-mCherry and EGFP-PICK1. Cells were single and cotransfected so that the protein dynamics could be compared when both proteins were present as evidence that the two proteins are associated. SH-SY5Y cells were also cotransfected with Arc-mCherry + EGFP or EGFP-PICK1 + mCherry to establish that an interaction between the protein of interest and the fluorescent tag was not occurring. PCH is a method used to determine fluorophore concentration and brightness in the cytosol[94]. Brightness is the counts per second per molecule in the sample, therefore when normalized to a monomeric standard represents average oligomerization state of the tagged protein. The brightness of Arc-mCherry in single transfected cells is not significantly different from that of Arc-mCherry cotransfected with EGFP, indicating that the presence of EGFP is not significantly affecting the brightness of Arc-mCherry (figure 8). In the presence of EGFP-PICK1, however, Arc-mCherry brightness is significantly increased compared to Arc-mCherry alone and trending toward significance compared to Arc-mCherry + EGFP (figure 8). Arc exists as a monomer alone and with EGFP but increases to an average normalized brightness of 1.37 in the presence of PICK1. The brightness of Arc-mCherry in the cytosol is relatively constant over a range of concentrations (figure 9). Therefore, the presence of PICK1 increases the self-association state of Arc. The oligomerization state of EGFP-PICK1 is between a monomer and a dimer and is not affected by cotransfection with Arc (figure 10) or concentration (figure 11).

In order to determine if Arc or PICK1 associate with large structures in the cytosol, we performed RICS on the single and cotransfected cells. RICS analysis gives the rate of diffusion and concentration of the fluorescent molecule[73]. If the proteins interact with cellular components, a decrease in the rate of diffusion will be observed. As expected, Arc-mCherry diffuses significantly slower than mCherry alone (figure 12). The diffusion of Arc-mCherry is not affected by cotransfection with EGFP or EGFP-PICK1 and does not show a clear trend in regard to concentration (figure 12 and figure 13). The diffusion of EGFP-PICK1 is also slower

than EGFP alone but is not affected by cotransfection with mCherry or Arc-mCherry (figure 14). EGFP-PICK1 diffusion in not affected by concentration (figure 15).

RICS signals can be cross-correlated between channels which allows us to determine if two fluorescent molecules are moving together and the diffusion of these molecules[95]. Two molecules moving together provides strong evidence that they are associated in some way. When cotransfected, Arc-mCherry and EGFP-PICK1 cross-correlate indicating that they are associated with each other in a complex in the cytosol. These complexes do not diffuse at a significantly different rate compared to Arc-mCherry or EGFP-PICK1 alone (figure 16). As a control, we cross-correlated the cells cotransfected with the secondary fluorescent protein (i.e. Arc-mCherry with EGFP and vice versa). We were not able to detect cross-correlation in these cells, indicating that the fluorescent tags are not causing the association.

3.2 Arc interacts with PICK1

To further support the evidence indicating that Arc associates with PICK1, we used FLIM to determine if we could observe FRET between EGFP-PICK1 and Arc-mCherry. For EGFP and mCherry the Förster critical distance has been reported as 52 Å at which 50% of the excitation energy will transfer from EGFP to mCherry[93]. FRET may occur if EGFP and mCherry are in very close proximity and in the proper orientation[59]. Therefore observation of FRET provides strong evidence that the two proteins are interacting. We used FLIM to determine if we could observe FRET from EGFP-PICK1 to Arc-mCherry. There was no significant difference in the average lifetime of EGFP-PICK1, which was consistent with the lifetime of EGFP alone (figure 17). The average lifetime for each cell was determined by averaging the τ_P with the τ_M for the center of the pixel distribution. Notably, the range of lifetime values for the cells cotransfected with EGFP-PICK1 and Arc-mCherry is larger than the range of the other groups. There were several cells in this condition with lower lifetime values that is likely due to FRET. It was interesting that a subset of the cotransfected cells had a lower lifetime while the majority of cells had a typical lifetime for EGFP. We wanted to determine what conditions could be causing Arc and PICK1 to interact more in some of the cells.

Chemical induction of LTD by glutamate is a commonly used technique. Addition of KCl to live cells is also frequently used to depolarize neuronal cells and has been shown to activate similar pathways as glutamate through NMDA receptor dependent processes[96,97]. In order to determine if Arc/PICK1 interaction is increased in LTD-inducing conditions, we incubated cotransfected cells in nondepolarizing buffer (low KCl) or depolarizing buffer (high KCl) prior to FLIM. The depolarizing buffer did not affect the lifetime of EGFP in life cells (Table 1). Two of ten cells transfected with EGFP-PICK1 alone had a set of pixels consistent with the lifetime of EGFP and second set of pixels with a lower lifetime. However, the pixels that were associated with the lower lifetime were distant from the cell and therefore did not appear to be originating from within the cell. Eighty percent of the cells that were cotransfected with EGFP-PICK1 and Arc-mCherry under nondepolarizing conditions had a single lifetime consistent with the lifetime of EGFP (figure 18). Additionally, twenty percent of the cells had a second set of pixels near or connected to the cell that exhibited a lower lifetime (Table 1). These pixels appeared to be in the projections of the neuronal-like cell, which would be biologically relevant to native dendritic activity of Arc. FRET was even more evident in the cotransfected cells that were depolarized as 12 of 17 cells had a second lower lifetime (Table 1). The second lifetime also appeared to exist in a projection of the cells (figure 19). This shows that depolarization contributes to the interaction of Arc and PICK1, which logically connects a mechanism from depolarization to AMPAR internalization through Arc/PICK1 association.

3.3 Arc/PICK1 brightness on the plasma membrane

Arc and PICK1 are associated with endocytosis of AMPARs[35,47], therefore we wanted to study the dynamics of these proteins at the plasma membrane. We used TIRF with N&B analysis to determine the molecular brightness at the membrane. N&B is used to determine the number of molecules in the excitation volume (N) and the brightness of the molecules at each pixel of a cell image[98]. As in PCH, when the brightness is normalized to a monomeric standard the value represents the average oligomerization state of the protein. We quantified the number of pixels that were associated with a monomer, dimer, of higher order brightness. For Arc-mCherry, there was no significant difference when co-transfected with EGFP-PICK1, with the

majority of pixels associated with a normalized brightness value between a monomer-dimer (1.49 ± 0.2). The median brightness for each cell shows a slight positive association with concentration (figure 21). At the membrane, EGFP-PICK1 has a median brightness value of a dimer (figure 22), which agrees with previous studies of PICK1 structure and function[49,99]. EGFP-PICK1 median normalized brightness was significantly higher than that of EGFP-PICK1 + mCherry or EGFP-PICK1 + Arc-mCherry (figure 22). However, none of the previous experiments indicated an effect of mCherry on EGFP-PICK1. There is no clear trend with concentration (figure 23). We think that the brightness difference may be due to the complexity of the cellular system and the overexpression of other proteins might mitigate fluctuations associated with higher order self-associations states of EGFP-PICK1 (such as tetramers).

Additionally, N&B analysis is not able to provide meaningful results on non-fluctuating structures such as endocytic puncta. We visually observed a difference in the presence of puncta at the membrane. Arc-mCherry alone typically forms large puncta on the membrane while EGFP-PICK1 does not (figure 24). However when coexpressed Arc-mCherry and EGFP-PICK1 formed large spots on the membrane that colocalized (figure 24). Puncta formation does not occur when Arc-mCherry is transfected with EGFP or when EGFP-PICK1 is cotransfected with mCherry. This supports evidence that Arc and PICK1 interact and that this interaction occurs at the membrane where there two proteins are natively active.

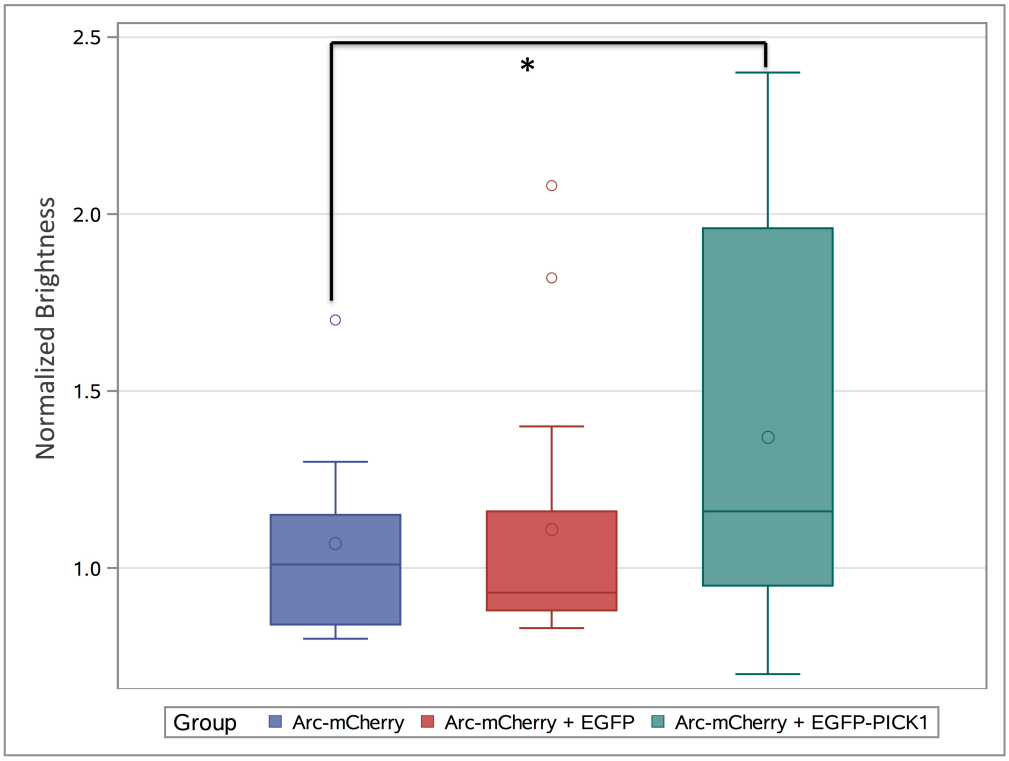

Figure 8. Normalized brightness of Arc-mCherry in the cytosol

Brightness values for Arc-mCherry normalized to mCherry in live cells. Cotransfection of EGFP-PICK1 with Arc-mCherry increases the brightness of Arc-mCherry alone (p=0.026). The normalized brightness of Arc-mCherry in the cotransfected cells is trending significantly higher compare to cells transfected with Arc-mCherry + EGFP (p=0.056). n=17-19 per group.

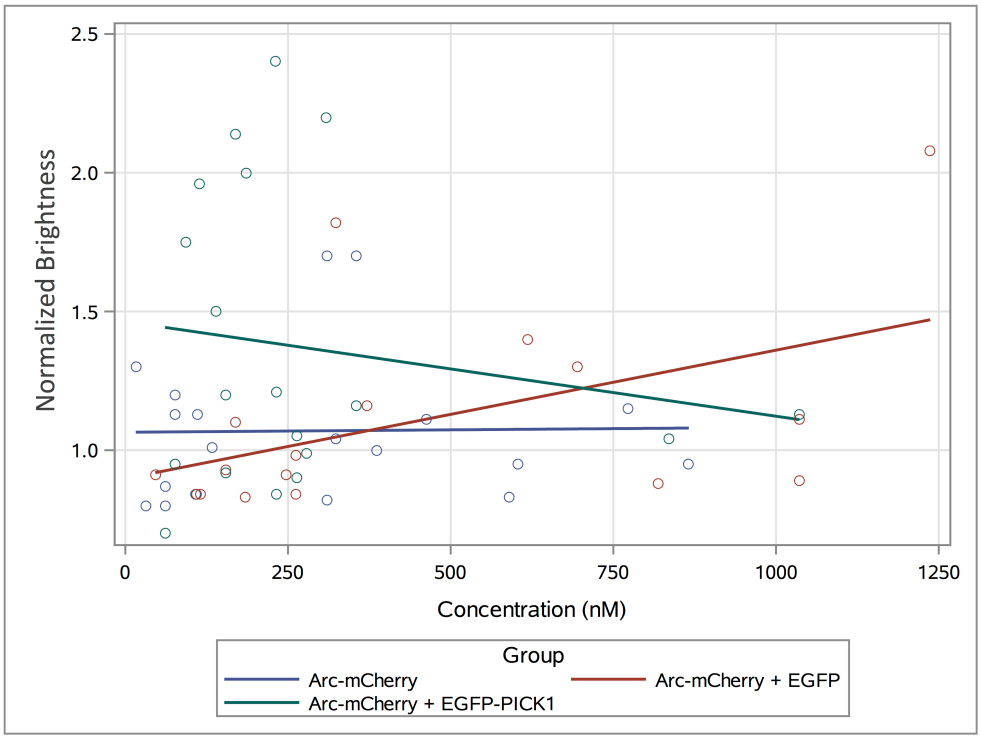

Figure 9. Concentration dependence of normalized brightness for Arc-mCherry in the cytosol

Arc-mCherry normalized brightness as a function of concentration.

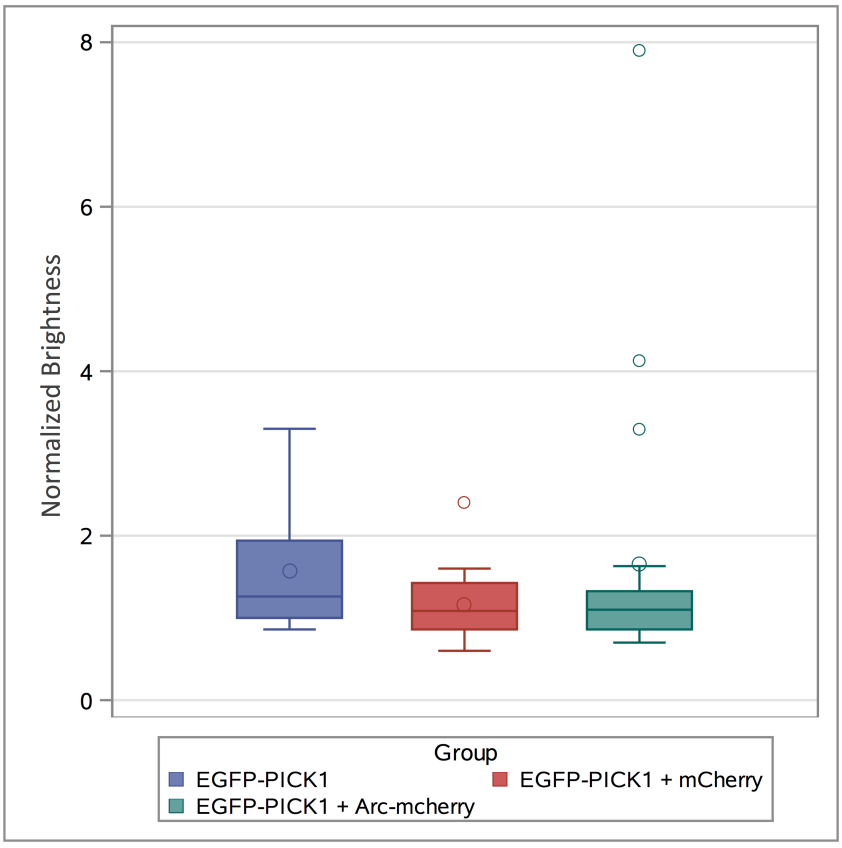

Figure 10. Normalized brightness of EGFP-PICK1 in the cytosol

Brightness values for EGFP-PICK1 normalized to EGFP in live cells. The normalized brightness between groups is not significantly different (One-Way ANOVA p=0.33, n=19-20 per group).

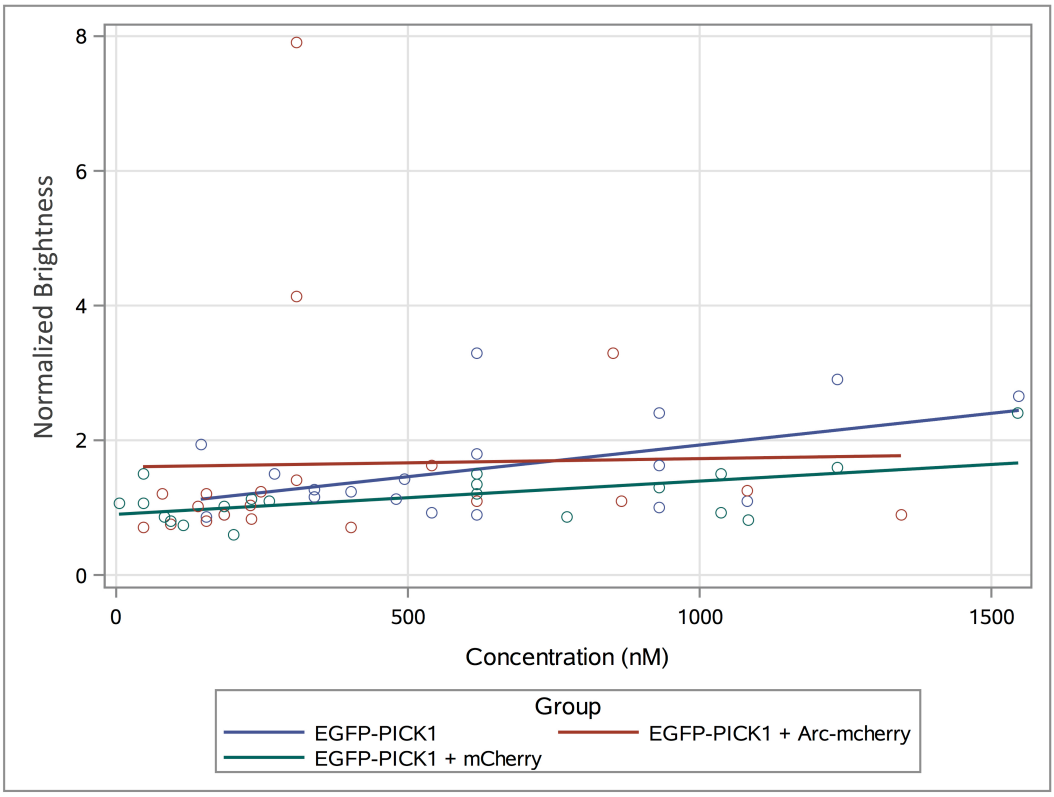

Figure 11. Concentration dependence of normalized brightness for EGFP-PICK1 in the cytosol

EGFP-PICK1 normalized brightness as a function of concentration.

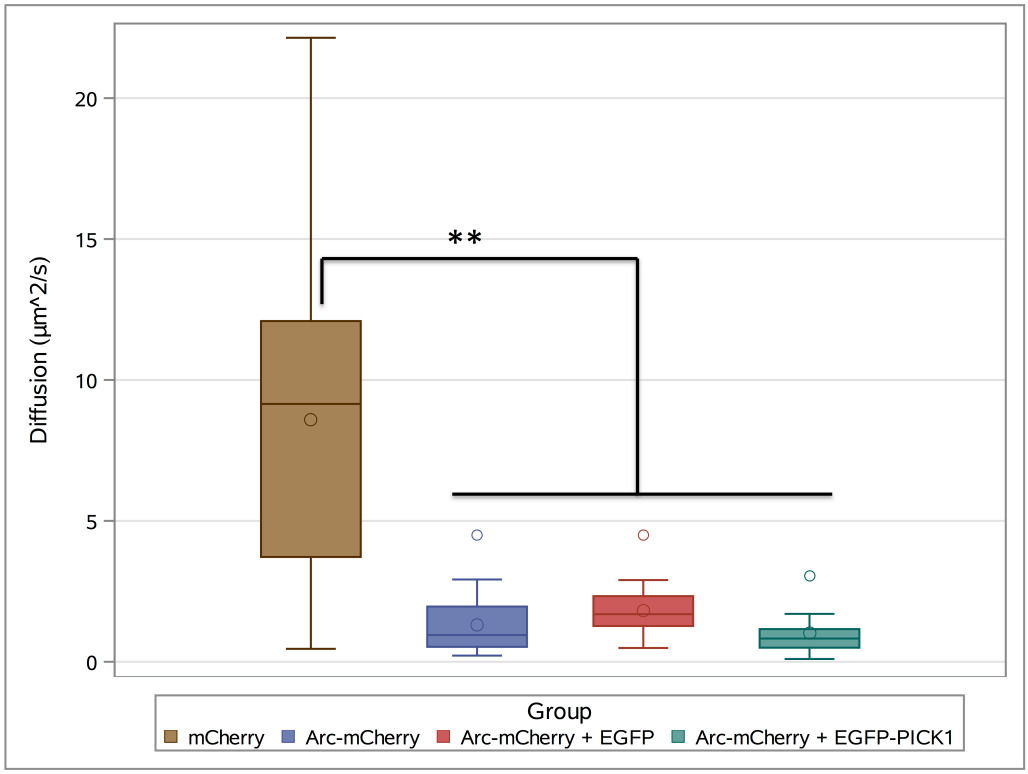

Figure 12. Diffusion of Arc-mCherry in the cytosol

Diffusion of mCherry in live cells is significantly higher than Arc-mCherry ($p<0.001$, n= 17-24 per group). The diffusion of Arc-mCherry between test conditions was not significantly different.

.

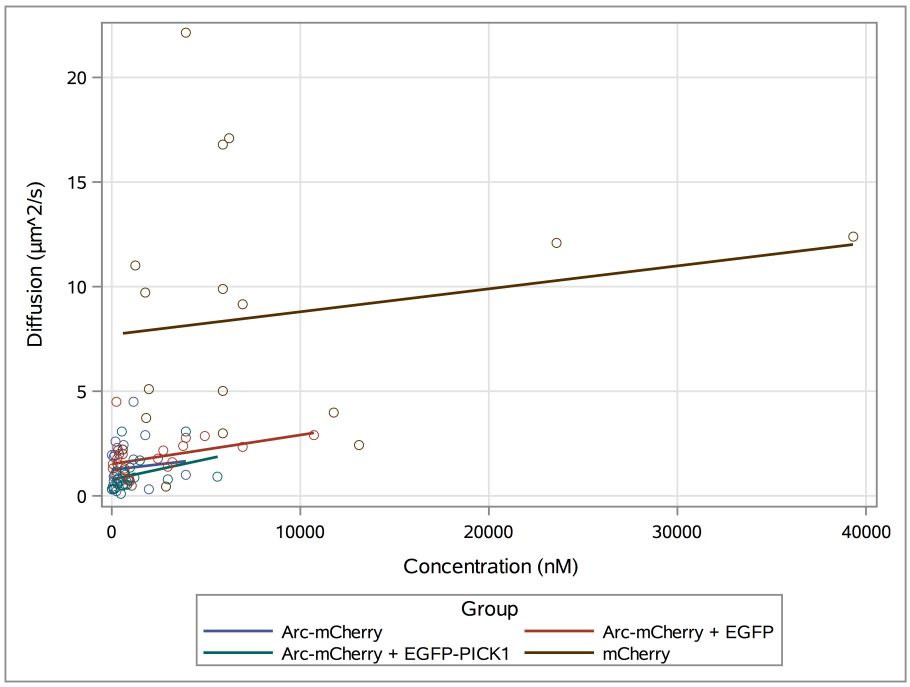

Figure 13. Concentration dependence of diffusion for mCherry and Arc-mCherry in the cytosol

mCherry and Arc-mCherry diffusion as a function of concentration.

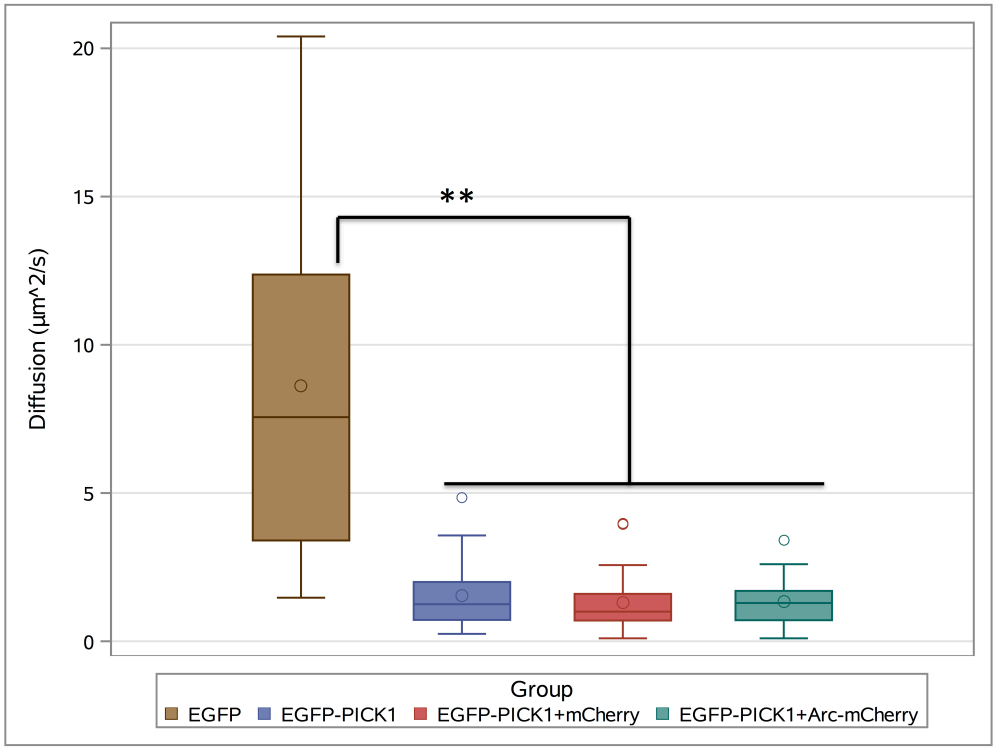

Figure 14. Diffusion of EGFP-PICK1 in the cytosol

Diffusion of EGFP in live cells is significantly higher than EGFP-PICK1 ($p<0.001$, n= 18-20 per group). The diffusion of EGFP-PICK1 between test conditions was not significantly different.

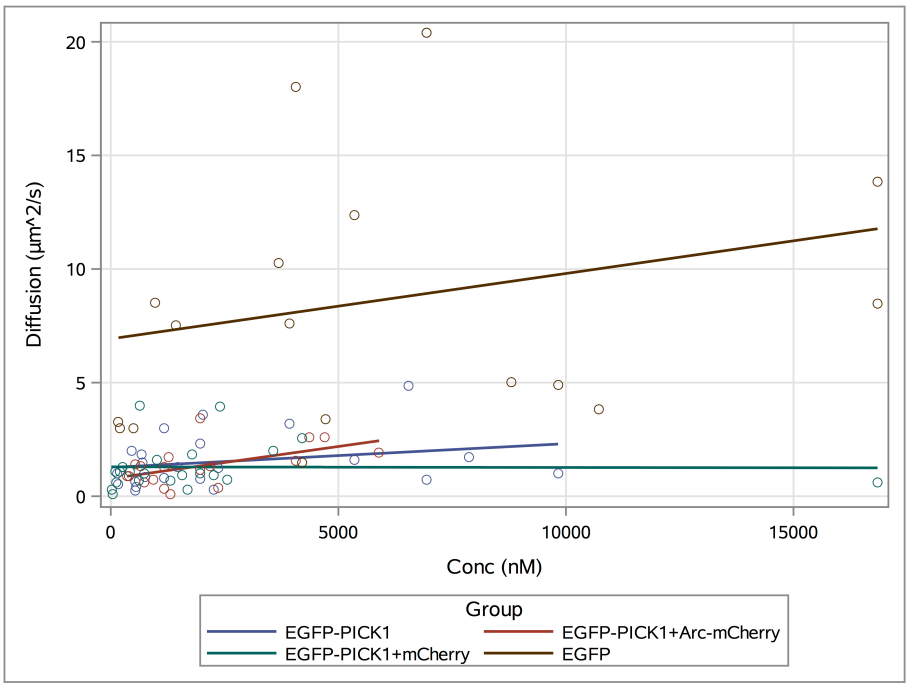

Figure 15. Concentration dependence of diffusion for EGFP and EGFP-PICK1 in the cytosol

EGFP and EGFP-PICK1 diffusion as a function of concentration.

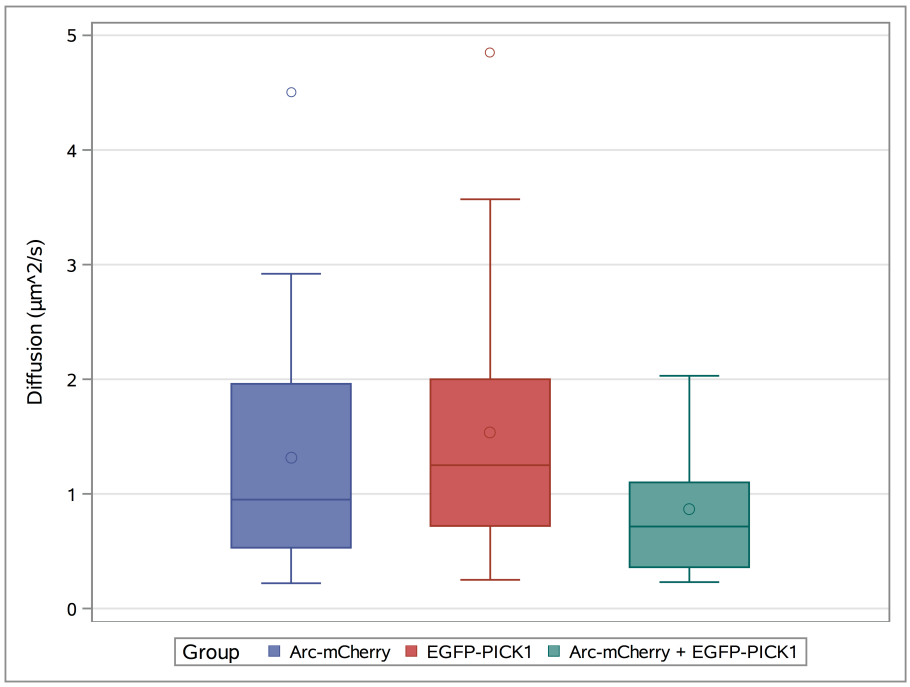

Figure 16. Diffusion of Arc-mCherry associated with EGFP-PICK1

Cross-correlation (green) of Arc-mCherry with EGFP-PICK1 in cotransfected cells demonstrates Arc-PICK1 interaction. The rate of diffusion of the cross-correlated species is not significantly different compared to the diffusion of Arc-mCherry or EGFP-PICK1 alone (One-Way ANOVA, p=0.25, n=10-24 per group).

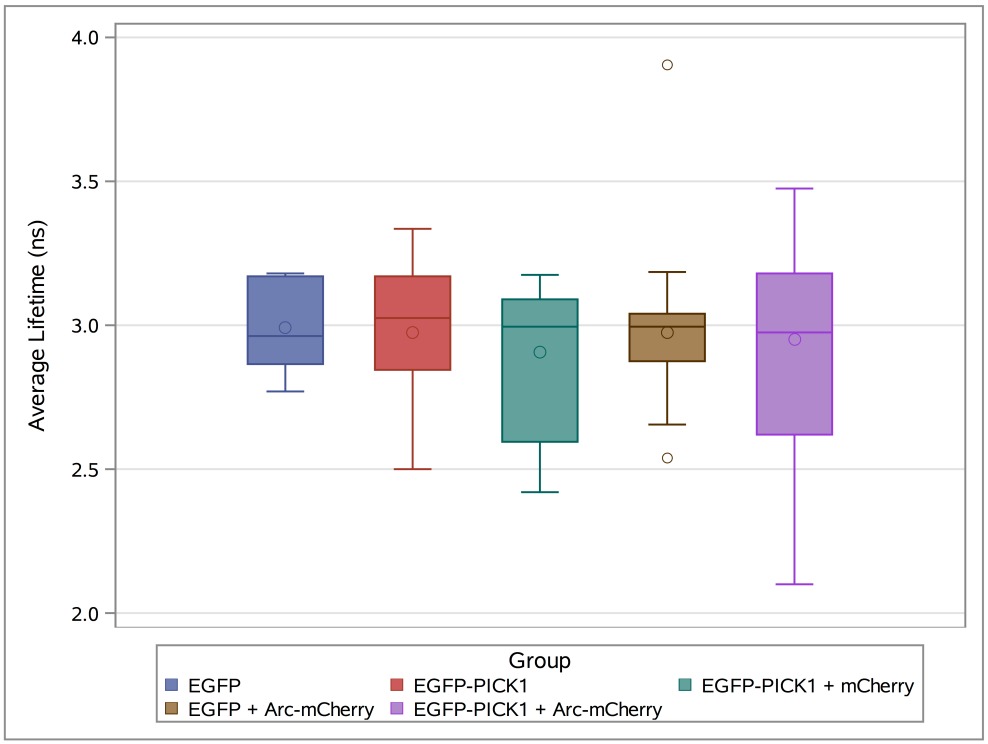

Figure 17. FRET shows evidence of interaction between Arc and PICK1

Fluorescence lifetime averaged between τ_P and τ_M for each cell. The lifetime is not significantly different between groups (One-Way ANOVA, p=0.85, n=16-23 per group). Though the average lifetime for the EGFP-PICK1 + Arc-mCherry group is not significantly different from that of the other groups the range of this group is larger than the other groups. There were several cells with lower lifetimes that were not observed in other groups.

Group	Depolarized	Average Lifetime (ns)	n	Average Lifetime (ns)	n
EGFP	N	2.41 ± 0.03	10		
EGFP	Y	2.43 ± 0.01	9		
PICK1	Y	2.40 ± 0.03	10	1.68 ± 0.05	2
EGFP-PICK1 + Arc-mCherry	N	2.38 ± 0.04	10	1.80 ± 0.01	2
EGFP-PICK1 + Arc-mCherry	Y	2.37 ± 0.05	17	1.85 ± 0.20	12

Table 1. Average fluorescence lifetimes in depolarized and nondepolarized cells

The average lifetime and standard deviation are presented for each group. If two lifetimes were present based on the phasor plot distribution a second average lifetime and standard deviation are presented along with the number of cells with a second lifetime.

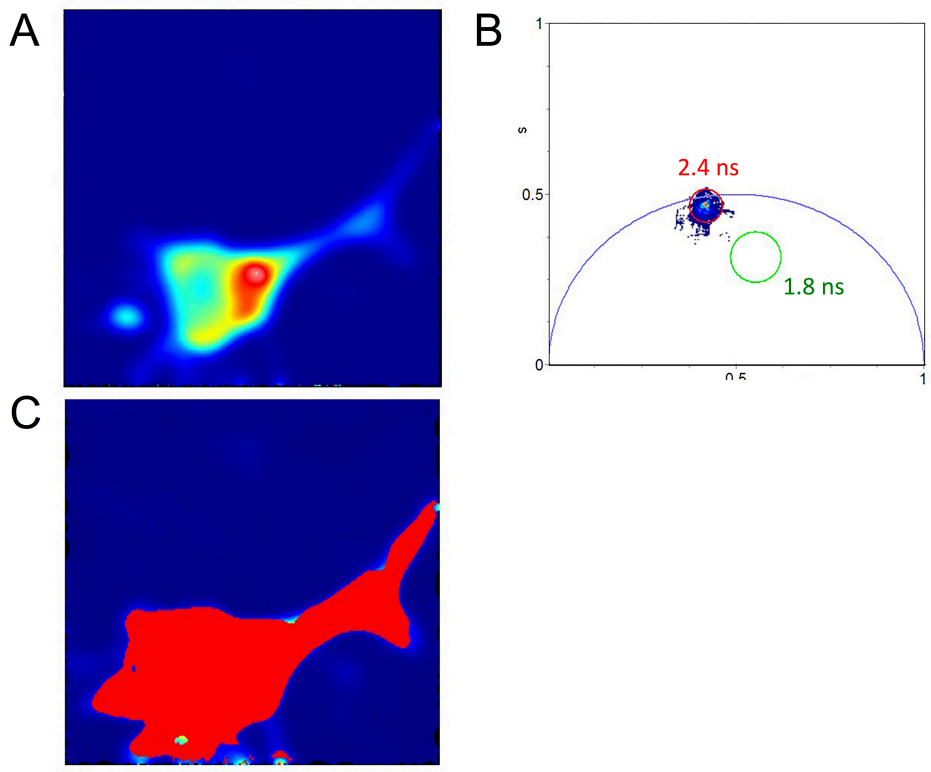

Figure 18. Nondepolarized cell with a single lifetime

A. Intensity image of a nondepolarized cell cotransfected with EGFP-PICK1 + Arc-mCherry. B. Phasor plot of the lifetime associated with the cell depicted. No points are seen in the green circle which represents a lifetime of 1.8ns. C. Cell image highlighted based on the lifetime. The red regions have a lifetime of approximately 2.4 ns, which are circled in red on panel B.

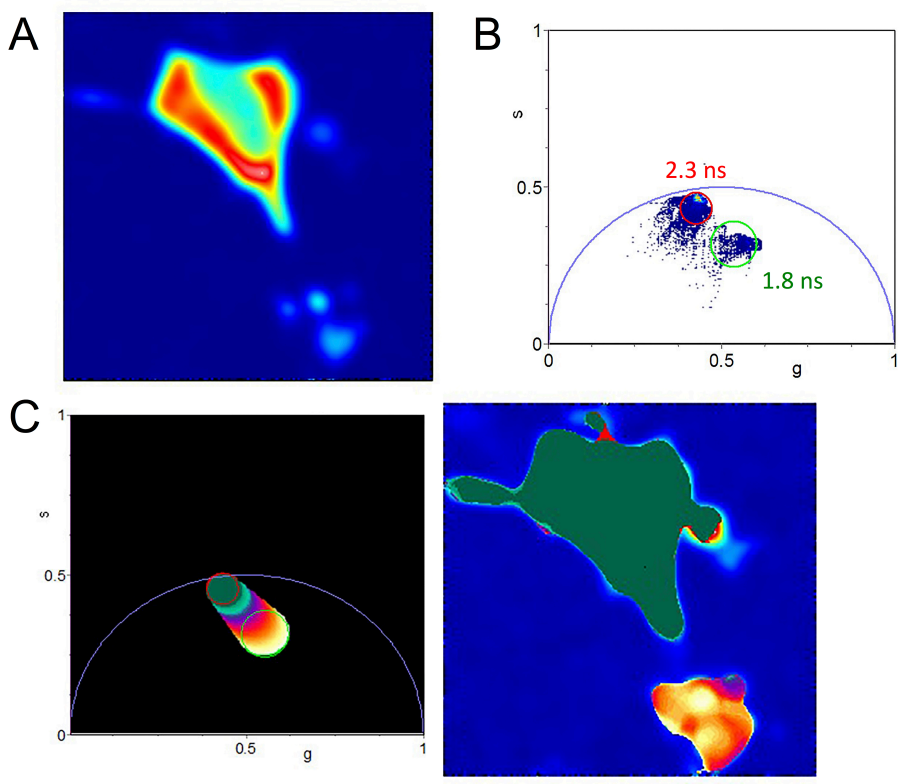

Figure 19. Depolarized cell demonstrating energy transfer

A. Intensity image of a depolarized cell cotransfected with EGFP-PICK1 + Arc-mCherry. B. Phasor plot of the lifetimes associated with the cell depicted. The red circle represents a lifetime of approximately 2.3ns and the green circle represents a lifetime of approximately 1.8ns. C. Cell image highlighted based on the lifetime. The left panel shows the color scheme used to illustrate the lifetime on the right panel. The projection area of the cell shows a lower lifetime compared to the cell body, likely due to energy transfer from EGFP to mCherry.

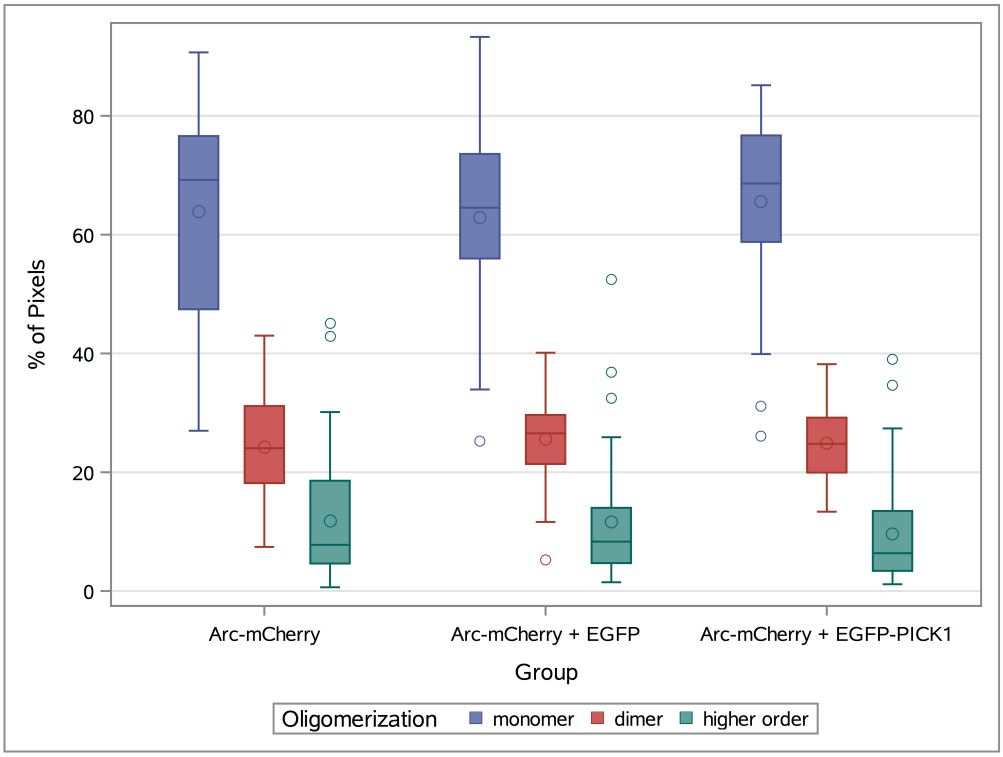

Figure 20. Normalized brightness of Arc-mCherry on the membrane

Percent of pixels of a cell that correspond to a normalized brightness value of monomer, dimer, or higher order oligomer is presented according to group. There is no significant difference between groups for any oligomerization state (One-Way ANOVA, p=0.61, n=43-58 per group).

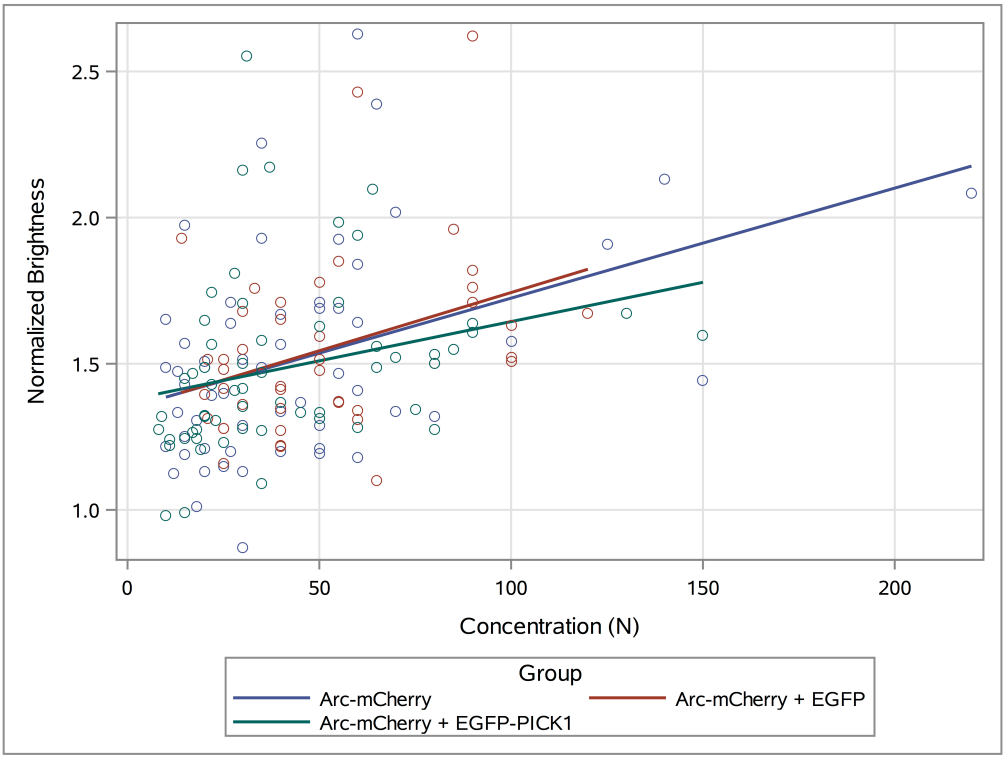

Figure 21. Concentration dependence of normalized brightness for Arc-mCherry on the membrane

Arc-mCherry median normalized brightness determined using TIRF microscopy as a function of concentration.

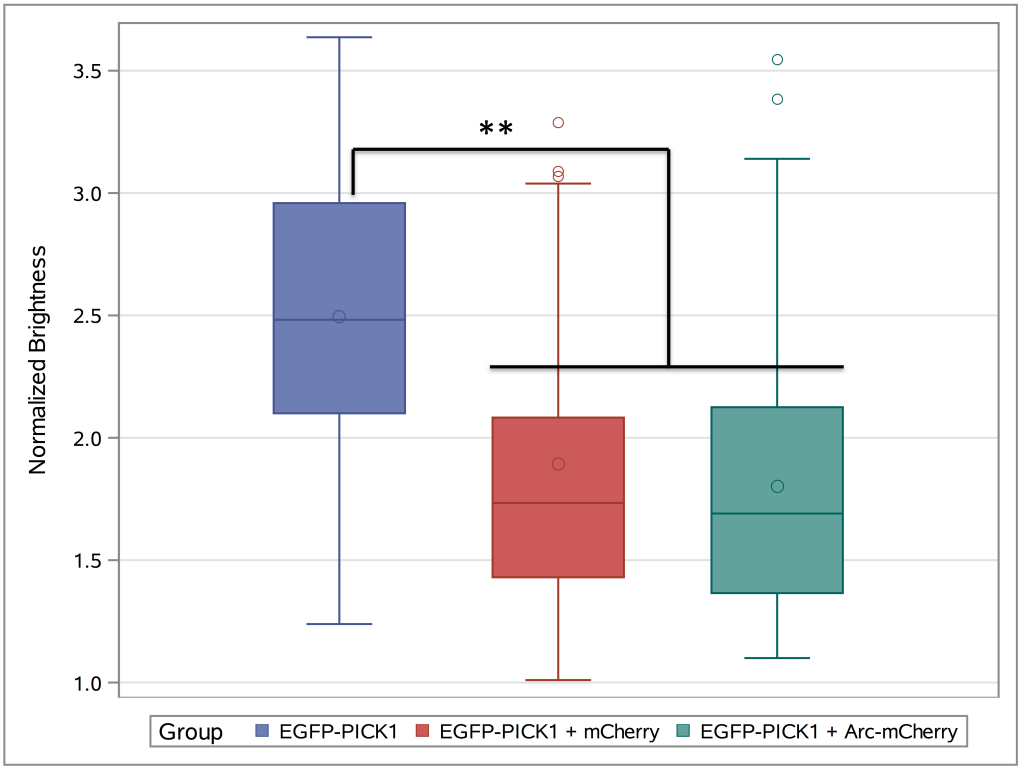

Figure 22. Normalized median brightness of EGFP-PICK1 on the membrane

The median normalized brightness of EGFP-PICK1 normalized to EGFP based on images collected using TIRF microscopy. The normalized brightness of EGFP-PICK1 is significantly higher than that of the cotransfected groups (One-Way ANOVA, $p<0.001$, n=54-68 per group).

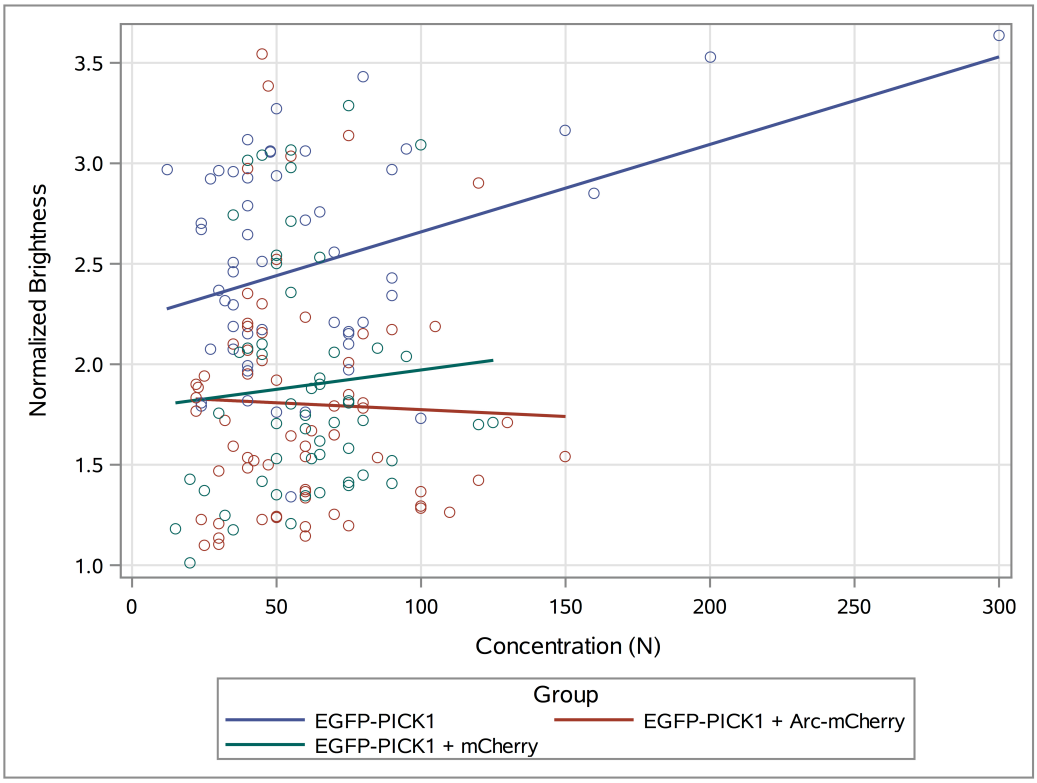

Figure 23. Concentration dependence of normalized brightness for EGFP-PICK1 on the membrane

EGFP-PICK1 normalized brightness determined using TIRF microscopy as a function of concentration.

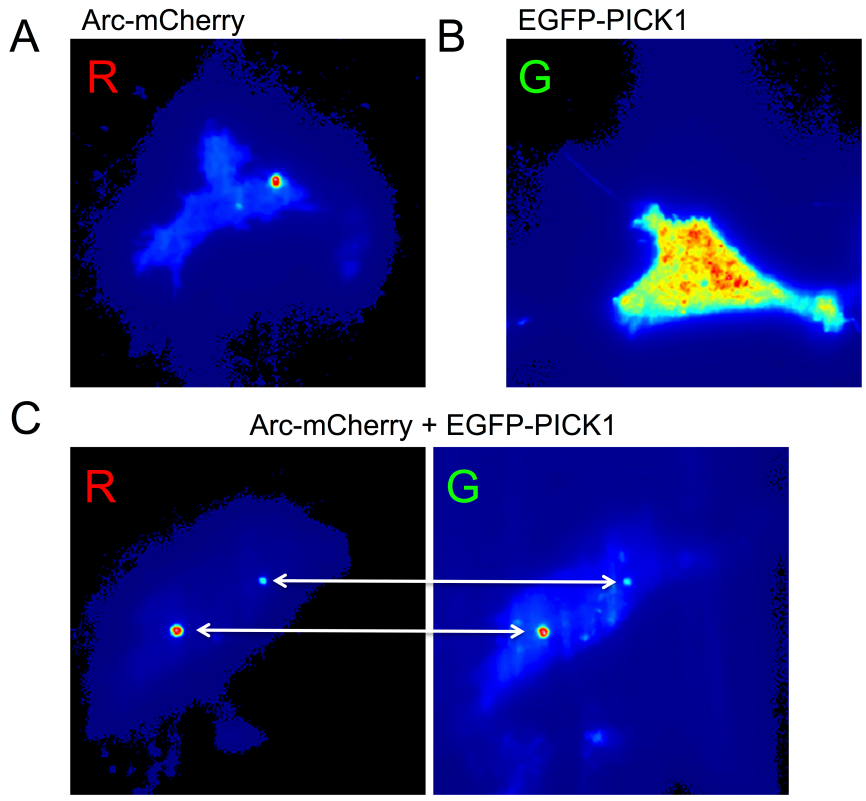

Figure 24. TIRF intensity images of transfected cells

A. Cell single transfected with Arc-mCherry showing large puncta. B. Cell single transfected with PICK1 that does not have puncta. C. Cell cotransfected with Arc-mCherry and EGFP-PICK1 that shows colocalized puncta in both the red and green channels.

CHAPTER 4. Discussion

4.1 Role of Arc/PICK1 interaction in learning and memory

Despite many studies on the function and regulation or Arc, a large gap has existed in the mechanism of specific AMPAR endocytosis associated with Arc expression. We sought to find a molecular connection between Arc and AMPARs through which Arc can facilitate trafficking of endocytic machinery. PICK1 was a good candidate for Arc interaction as it is known to bind to the C-terminal tail of AMPARs and is associated with AMPAR trafficking during LTD[100]. In this study, we demonstrated that Arc interacts with PICK1 wherein there is a marked promotion in PICK1 clustering on the plasma membrane. In addition, we have shown that this interaction is primarily observed towards the projects of SH-SY5Y cells and is enhanced under depolarizing conditions. This localization in interaction suggests that these sites contain signals required to facilitate Arc-PICK1 interaction. Additionally, there may be intracellular signals that are activated during depolarization that affect the affinity of Arc and PICK1. Of interest, we noticed a concentration dependence of Arc self-association on the plasma membrane (figure 21). Therefore, it is possible that rapid expression of Arc during LTD increases the local concentration to promote protein association. It has been shown that the presence of Arc increases dynamin polymerization and GTPase activity[45]. Therefore Arc can greatly facilitate the rate of endocytosis through the activity of dynamin. This activity will specifically occur near AMPARs due to Arc/PICK1 interaction.

We characterized the biophysical properties of Arc and PICK1 in the cytosol and at the plasma membrane of SH-SY5Y cells. Within the cytosol both molecules had reduced diffusion indicating that the mobile fraction of these proteins were associated with slower moving cellular components. Brightness analysis demonstrates that Arc is primarily monomeric while PICK1 exists as a monomer-dimer equilibrium. Cross-correlation of the RICS images for Arc-PICK1 indicate that their interaction in the cytosol is occurring on slow moving structures as the diffusion is not significantly altered. Moreover, the B values seem to indicate that the interaction of these two proteins could be on the order of 1:1 or 1:2 (Arc:PICK1). Both potentially would work biologically as one could envision an arrangement where PICK1 binding

occurs between AMPARs and Arc. However, the specific stoichiometries of these interactions remain to be determined.

Arc and PICK1 activity are associated on the plasma membrane. Therefore, we anticipated significant alterations in protein dynamics when examining the plasma membrane via TIRF microscopy. Interestingly, we found no significant change in brightness values between cytosol and the plasma membrane. However, we observed large spots of Arc and PICK1 on the plasma membrane when cotransfected, which due to slow mobility are difficult to include in N&B values because the intensity variance is low. The size of these aggregates are much larger than puncta that are typically associated with clathrin-mediated endocytosis which are at or below the point spread function of our microscope[101]. Therefore, these aggregates may serve as a protein hub to prepare for endocytosis.

Over the past decade, several laboratories have discovered interactions between Arc and other proteins. This list includes dynamin[44], endophilin[44], clathrin-adaptor protein 2[102], possibly TARPγ2 (Stargazin)[103], and now PICK1. The three dimensional structure of Arc, however, has few identifiable domains. Given the interaction of Arc with numerous proteins we postulate that Arc acts as a scaffolding protein during LTD. Our results suggest that LTD-induced reduction in surface AMPARs results from Arc scaffolding between PICK1 bound to GluR2 or GluR3 and the endocytic machinery (endophilin, dynamin, and clathrin). Arc thereby directs the targeting of endocytic machinery to AMPARs to reduce surface expression.

4.2 Future directions

Depolarization was shown to increase the interaction of Arc and PICK1, which verifies a promising role of the interaction in LTD. KCl depolarization has been shown to bring about similar molecular effects compared to chemical induction of LTD by low dose NMDA[96]. However, there are two distinct types of LTD in hippocampal CA1 cells, NMDAR-dependent and mGluR-dependent. Therefore different chemical induction protocols for LTD exist by the addition of glutamate[41], NMDA[96], or DHPG which is selective for mGluRs[104]. It will be important to delineate if there is a difference in Arc/PICK1 interaction under various conditions of LTD induction to establish its role in different mechanisms of LTD. Additionally, Arc/PICK1

interaction studies should be conducted with varying levels of calcium and PKC as these are important intracellular signaling molecules that are associated with LTD.

Without a method to manipulate the Arc/PICK1 interaction it will be difficult to establish the role of the interaction in LTD. Both proteins are individually associated with AMPAR endocytosis but whether an interaction between them is required is not known. Efforts to isolate and mutate the binding regions of the protein are therefore needed. Additionally, it has been shown that Arc is no longer functional in recovering memory deficits in mice when tagged with a fluorescent protein (Kimberly Huber, unpublished). We are currently working on developing a model to tag this protein with a fluorescent molecule that will not impact its function. Ultimately, we hope that uncovering the molecular mechanism of Arc in LTD will help us understand and direct treatments for diseases associated with altered expression of Arc.

REFERENCES

1. Isaac JTR, Ashby MC, McBain CJ. The Role of the GluR2 Subunit in AMPA Receptor Function and Synaptic Plasticity. *Neuron*. 2007;54(6):859-871. doi:10.1016/j.neuron.2007.06.001.
2. Shepherd JD, Huganir RL. The Cell Biology of Synaptic Plasticity: AMPA Receptor Trafficking. *Annu Rev Cell Dev Biol*. 2007;23:613-643. doi:10.1146/annurev.cellbio.23.090506.123516.
3. Greger IH, Ziff EB, Penn AC, et al. Molecular determinants of AMPA receptor subunit assembly. *Trends Neurosci*. 2007;30(8):407-416. doi:10.1016/j.tins.2007.06.005.
4. Bredt DS, Nicoll RA. AMPA Receptor Trafficking at Excitatory Synapses. *Neuron*. 2003;40(2):361-379. doi:10.1016/S0896-6273(03)00640-8.
5. Penn AC, Williams SR, Greger IH, et al. Gating motions underlie AMPA receptor secretion from the endoplasmic reticulum. *EMBO J*. 2008;27(22):3056-3068. doi:10.1038/emboj.2008.222.
6. Ju W, Morishita W, Tsui J, et al. Activity-dependent regulation of dendritic synthesis and trafficking of AMPA receptors. *Nat Neurosci*. 2004;7(3):244-253. doi:10.1038/nn1189.
7. Borgdorff AJ, Choquet D. Regulation of AMPA receptor lateral movements. *Nature*. 2002;417(6889):649-653. doi:10.1038/nature00780.
8. Choquet D, Triller A. The role of receptor diffusion in the organization of the postsynaptic membrane. *Nat Rev Neurosci*. 2003;4(4):251-265. doi:10.1038/nrn1077.
9. Passafaro M, Piëch V, Sheng M. Subunit-specific temporal and spatial patterns of AMPA receptor exocytosis in hippocampal neurons. *Nat Neurosci*. 2001;4(9):917-926. doi:10.1038/nn0901-917.
10. Piccini A, Malinow R. Critical Postsynaptic Density 95/Disc Large/Zonula Occludens-1 Interactions by Glutamate Receptor 1 (GluR1) and GluR2 Required at Different Subcellular Sites. *J Neurosci*. 2002;22(13):5387-5392.
11. Lu W, Man H, Ju W, et al. Activation of synaptic NMDA receptors induces membrane insertion of new AMPA receptors and LTP in cultured hippocampal neurons. *Neuron*. 2001;29(1):243-254. doi:10.1016/S0896-6273(01)00194-5.
12. Lee SH, Valtschanoff JG, Kharazia VN, Weinberg R, Sheng M. Biochemical and

morphological characterization of an intracellular membrane compartment containing AMPA receptors. *Neuropharmacology*. 2001;41(6):680-692. http://www.ncbi.nlm.nih.gov/pubmed/11640922. Accessed February 4, 2017.

13. Nabavi S, Fox R, Proulx CD, Lin JY, Tsien RY, Malinow R. Engineering a memory with LTD and LTP. *Nature*. 2014;511. doi:10.1038/nature13294.
14. Lü Scher C, Malenka RC. NMDA Receptor-Dependent Long-Term Potentiation and Long-Term Depression (LTP/LTD). *Cold Spring Harb Perspect Biol*. 2012;4a005710. doi:10.1101/cshperspect.a005710.
15. Lüscher C, Huber KM. Group 1 mGluR-dependent synaptic long-term depression (mGluR-LTD): mechanisms and implications for circuitry & disease Cellular mechanisms of Group 1 mGluR-dependent synaptic plasticity. *Neuron*. 2010;65(4):445-459. doi:10.1016/j.neuron.2010.01.016.
16. Niswender CM, Conn PJ. Metabotropic Glutamate Receptors: Physiology, Pharmacology, and Disease. *Annu Rev Pharmacol Toxicol*. 2010;50:295-322. doi:10.1146/annurev.pharmtox.011008.145533.
17. Monfils M-H, Teskey GC. Induction of long-term depression is associated with decreased dendritic length and spine density in layers III and V of sensorimotor neocortex. *Synapse*. 2004;53(2):114-121. doi:10.1002/syn.20039.
18. Zhou Q, Homma KJ, Poo M-M. Report Shrinkage of Dendritic Spines Associated with Long-Term Depression of Hippocampal Synapses. *Neuron*. 2004;44:749-757. doi:10.1016/j.neuron.2004.11.011.
19. Lamprecht R, LeDoux J. Structural plasticity and memory. *Nat Rev Neurosci*. 2004;5(1):45-54. doi:10.1038/nrn1301.
20. Derkach VA, Oh MC, Guire ES, Soderling TR. Regulatory mechanisms of AMPA receptors in synaptic plasticity. *Nat Rev Neurosci*. 2007;8(2):101-113. doi:10.1038/nrn2055.
21. Malenka RC, Bear MF. Review LTP and LTD: An Embarrassment of Riches useful to conceptualize LTP and LTD as a general class of cellular/synaptic phenomena. Just as different neu- rons express different complements of ion channels to. *Neuron*. 2004;44:5-21.

22. Ashby MC, De La Rue SA, Ralph GS, Uney J, Collingridge GL, Henley JM. Removal of AMPA Receptors (AMPARs) from Synapses Is Preceded by Transient Endocytosis of Extrasynaptic AMPARs. *J Neurosci*. 2004;24(22):5172-5176. doi:10.1523/JNEUROSCI.1042-04.2004.
23. Kim E, Sheng M. PDZ domain proteins of synapses. *Nat Rev Neurosci*. 2004;5(10):771-781. doi:10.1038/nrn1517.
24. Tomita S, Nicoll RA, Bredt DS. PDZ protein interactions regulating glutamate receptor function and plasticity. *J Cell Biol*. 2001;153(5):F19-24. http://www.ncbi.nlm.nih.gov/pubmed/11381098. Accessed January 29, 2017.
25. McGlade-McCulloh E, Yamamoto H, Tan S-E, Brickey DA, Soderling TR. Phosphorylation and regulation of glutamate receptors by calcium/calmodulin-dependent protein kinase II. *Nature*. 1993;362(6421):640-642. doi:10.1038/362640a0.
26. Yin HH, Davis MI, Ronesi JA, Lovinger DM. The Role of Protein Synthesis in Striatal Long-Term Depression. *J Neurosci*. 2006;26(46):11811-11820. doi:10.1523/JNEUROSCI.3196-06.2006.
27. Lyford GL, Yamagata K, Kaufmann WE, et al. Arc, a growth factor and activity-regulated gene, encodes a novel cytoskeleton-associated protein that is enriched in neuronal dendrites. *Neuron*. 1995;14(2):433-445. doi:10.1016/0896-6273(95)90299-6.
28. Plath N, Ohana O, Dammermann B, et al. *Arc/Arg3.1 Is Essential for the Consolidation of Synaptic Plasticity and Memories*. Vol 52.; 2006. doi:10.1016/j.neuron.2006.08.024.
29. Fletcher BR, Hill GS, Long JM, Gallagher M, Shapiro ML, Rapp PR. A fine balance: Regulation of hippocampal Arc/Arg3.1 transcription, translation and degradation in a rat model of normal cognitive aging. *Neurobiol Learn Mem*. 2014;115:58-67. doi:10.1016/j.nlm.2014.08.007.
30. Kerrigan TL, Randall AD. A New Player in the "Synaptopathy" of Alzheimer's Disease – Arc/Arg 3.1. *Front Neurol*. 2013;4:9. doi:10.3389/fneur.2013.00009.
31. Purcell SM, Moran JL, Fromer M, et al. A polygenic burden of rare disruptive mutations in schizophrenia. *Nature*. 2014;506:185-190. doi:10.1038/nature12975.
32. Fromer M, Pocklington AJ, Kavanagh DH, et al. De novo mutations in schizophrenia implicate synaptic networks. *Nature*. 2014;506:179-184. doi:10.1038/nature12929.

33. Niere F, Wilkerson JR, Huber KM. Evidence for a Fragile X Mental Retardation Protein-Mediated Translational Switch in Metabotropic Glutamate Receptor-Triggered Arc Translation and Long-Term Depression. *J Neurosci*. 2012;32(17):5924-5936. doi:10.1523/JNEUROSCI.4650-11.2012.

34. Greer PL, Hanayama R, Bloodgood BL, et al. The Angelman Syndrome Protein Ube3A Regulates Synapse Development by Ubiquitinating Arc. *Cell*. 2010;140(5):704-716. doi:10.1016/j.cell.2010.01.026.

35. Bramham CR, Alme MN, Bittins M, et al. The Arc of synaptic memory. *Exp Brain Res*. 2010:125-140. doi:10.1007/s00221-009-1959-2.

36. Jakkamsetti V, Tsai N-P, Gross C, et al. *Experience-Induced Arc/Arg3.1 Primes CA1 Pyramidal Neurons for Metabotropic Glutamate Receptor-Dependent Long-Term Synaptic Depression*. Vol 80.; 2013. doi:10.1016/j.neuron.2013.07.020.

37. Steward O, Wallace CS, Lyford GL, Worley PF. Synaptic activation causes the mRNA for the IEG Arc to localize selectively near activated postsynaptic sites on dendrites. *Neuron*. 1998;21(4):741-751. doi:10.1016/S0896-6273(00)80591-7.

38. Link W, Konietzko U, Kauselmann G, et al. Somatodendritic expression of an immediate early gene is regulated by synaptic activity (hippocampus/neuronal plasticity/seizure/long-term potentiation/gene induction). *Neurobiology*. 1995;92:5734-5738.

39. Farris S, Lewandowski G, Cox CD, Steward O. Selective localization of arc mRNA in dendrites involves activity- and translation-dependent mRNA degradation. *J Neurosci*. 2014;34(13):4481-4493. doi:10.1523/JNEUROSCI.4944-13.2014.

40. Moga DE, Calhoun ME, Chowdhury A, Worley P, Morrison JH, Shapiro ML. *Activity-Regulated Cytoskeletal-Associated Protein Is Localized to Recently Activated Excitatory Synapses*. Vol 125.; 2004. doi:10.1016/j.neuroscience.2004.02.004.

41. Na Y, Park S, Lee C, et al. Real-Time Imaging Reveals Properties of Glutamate-Induced Arc/Arg 3.1 Translation in Neuronal Dendrites. *Neuron*. 2016;91(3):561-573. doi:10.1016/j.neuron.2016.06.017.

42. Shepherd JD, Rumbaugh G, Wu J, et al. Arc/Arg3.1 Mediates Homeostatic Synaptic Scaling of AMPA Receptors. *Neuron*. 2006;52(3):475-484. doi:10.1016/j.neuron.2006.08.034.

43. Waung MW, Pfeiffer BE, Nosyreva ED, Ronesi JA, Huber KM. Rapid Translation of Arc/Arg3.1 Selectively Mediates mGluR-Dependent LTD through Persistent Increases in AMPAR Endocytosis Rate. *Neuron*. 2008;59:84-97. doi:10.1016/j.neuron.2008.05.014.
44. Chowdhury S, Shepherd JD, Okuno H, et al. Arc/Arg3.1 Interacts with the Endocytic Machinery to Regulate AMPA Receptor Trafficking. *Neuron*. 2006;52(3):445-459. doi:10.1016/j.neuron.2006.08.033.
45. Byers CE, Barylko B, Ross JA, et al. Enhancement of dynamin polymerization and GTPase activity by Arc/Arg3.1. *Biochim Biophys Acta - Gen*. 2015;1850(6):1310-1318. doi:10.1016/j.bbagen.2015.03.002.
46. Zhang W, Wu J, Leahy DJ, et al. Structural Basis of Arc Binding to Synaptic Proteins: Implications for Cognitive Disease. *Neuron*. 2015;86:490-500. doi:10.1016/j.neuron.2015.03.030.
47. Li Y-H, Zhang N, Wang Y-N, Shen Y, Wang Y. Multiple faces of protein interacting with C kinase 1 (PICK1): Structure, function, and diseases. *Neurochem Int*. 2016. doi:10.1016/j.neuint.2016.03.001.
48. He Y, Liwo A, Weinstein H, Scheraga HA. PDZ Binding to the BAR Domain of PICK1 is Elucidated by Coarse-grained Molecular Dynamics. *J Mol Biol*. 2011;405(1):298-314. doi:10.1016/j.jmb.2010.10.051.
49. Karlsen MLL, Thorsen TSS, Johner N, et al. Structure of Dimeric and Tetrameric Complexes of the BAR Domain Protein PICK1 Determined by Small-Angle X-Ray Scattering. *Structure*. 2015;23(7):1258-1270. doi:10.1016/j.str.2015.04.020.
50. Xia J, Zhang X, Staudinger J, Huganir RL. Clustering of AMPA Receptors by the Synaptic PDZ Domain–Containing Protein PICK1. *Neuron*. 1999;22(1):179-187. doi:10.1016/S0896-6273(00)80689-3.
51. Dev KK, Nishimune A, Henley JM, Nakanishi S. The protein kinase Cα binding protein PICK1 interacts with short but not long form alternative splice variants of AMPA receptor subunits. *Neuropharmacology*. 1999;38(5):635-644. doi:10.1016/S0028-3908(98)00230-5.
52. Lè Ne Hirbec H, Perestenko O, Nishimune A, et al. The PDZ Proteins PICK1, GRIP, and Syntenin Bind Multiple Glutamate Receptor Subtypes ANALYSIS OF PDZ BINDING

MOTIFS*. *J Biol Chem*. 2002;277:15221-15224. doi:10.1074/jbc.C200112200.

53. Xia J, Chung HJ, Wihler C, Huganir RL, Linden DJ. Cerebellar Long-Term Depression Requires PKC-Regulated Interactions between GluR2/3 and PDZ Domain–Containing Proteins. *Neuron*. 2000;28(2):499-510. doi:10.1016/S0896-6273(00)00128-8.
54. Chung HJ, Xia J, Scannevin RH, Zhang X, Huganir RL. Phosphorylation of the AMPA Receptor Subunit GluR2 Differentially Regulates Its Interaction with PDZ Domain-Containing Proteins. *J Neurosci*. 2000;20(19):7258-7267.
55. Newton AC. Protein kinase C: structure, function, and regulation. *J Biol Chem*. 1995;270(48):28495-28498. doi:10.1074/JBC.270.48.28495.
56. Hanley JG, Henley JM. PICK1 is a calcium-sensor for NMDA-induced AMPA receptor trafficking. *EMBO J*. 2005;24(18):3266-3278. doi:10.1038/sj.emboj.7600801.
57. Citri A, Bhattacharyya S, Ma C, et al. Calcium binding to PICK1 is essential for the intracellular retention of AMPA receptors underlying long-term depression. *J Neurosci*. 2010;30(49):16437-16452. doi:10.1523/JNEUROSCI.4478-10.2010.
58. Jo J, Heon S, Kim MJ, et al. Metabotropic glutamate receptor-mediated LTD involves two interacting Ca(2+) sensors, NCS-1 and PICK1. *Neuron*. 2008;60(6):1095-1111. doi:10.1016/j.neuron.2008.10.050.
59. Jameson DM. *Introduction to Fluorescence*. Boca Raton: Taylor & Francis Group; 2014.
60. Valeur B, Berberan-Santos MN. *Molecular Fluorescence: Principles and Applications*. 2nd ed. Wheinheim: Wiley-VCH; 2012.
61. Amos WB, White JG. How the Confocal Laser Scanning Microscope entered Biological Research. *Biol Cell*. 2003;95:335-342. doi:10.1016/S0248-4900(03)00078-9.
62. Paddock SW, Eliceiri KW. Laser Scanning Confocal Microscopy: History, Applications, and Related Optical Sectioning Techniques. In: *Methods in Molecular Biology*. Vol 1075. New York: Springer Science and Business Media; 2014:9-47. doi:10.1007/978-1-60761-847-8_2.
63. Mattheyses AL, Simon SM, Rappoport JZ. Imaging with total internal reflection fluorescence microscopy for the cell biologist. *J Cell Sci*. 2010;123:3621-3628. doi:10.1083/jcb.200903097.
64. Schneckenburger H. Total internal reflection fluorescence microscopy: technical

innovations and novel applications. *Curr Opin Biotechnol*. 2005;16:13-18. https://www.researchgate.net/profile/Herbert_Schneckenburger/publication/8011467_Total_internal_reflection_fluorescence_microscopy_Technical_innovations_and_novel_applications/links/0912f50e5477a6440c000000/Total-internal-reflection-fluorescence-microscop. Accessed March 14, 2017.

65. Axelrod D. Total Internal Reflection Fluorescence Microscopy in Cell Biology. *Traffic*. 2001;2(11):764-774. doi:10.1034/j.1600-0854.2001.21104.x.
66. Martin-Fernandez ML, Tynan CJ, Webb SED. A "pocket guide" to total internal reflection fluorescence. *J Microsc*. 2013;252(1):16-22. doi:10.1111/jmi.12070.
67. So PTC, Dong CY, Masters BR, Berland KM. Two-Photon Excitation Fluorescence Microscopy. *Annu Rev Biomed Eng*. 2000;2:399-429. http://light.ece.illinois.edu/ECE564/Research_Projects_files/TPFM_annurev.bioeng.2.1.pdf. Accessed March 5, 2017.
68. Oheim M, Michael DJ, Geisbauer M, Madsen D, Chow RH. Principles of two-photon excitation fluorescence microscopy and other nonlinear imaging approaches. *Adv Drug Deliv Rev*. 2006;58:788-808. doi:10.1016/j.addr.2006.07.005.
69. Svoboda K, Yasuda R. Principles of Two-Photon Excitation Microscopy and Its Applications to Neuroscience. *Neuron*. 2006;50:823-839. doi:10.1016/j.neuron.2006.05.019.
70. Magidson V, Khodjakov A. Circumventing photodamage in live-cell microscopy. *Methods Cell Biol*. 2013;114. doi:10.1016/B978-0-12-407761-4.00023-3.
71. Chen Y, Müller JD, Berland KM, Gratton E. Fluorescence Fluctuation Spectroscopy. *Methods*. 1999;19(2):234-252. doi:10.1006/meth.1999.0854.
72. Jameson DM, Ross JA, Albanesi JP. Fluorescence fluctuation spectroscopy: ushering in a new age of enlightenment for cellular dynamics. *Biophys Rev*. 2009;1(3):105-118. doi:10.1007/s12551-009-0013-8.
73. Rossow MJ, Sasaki JM, Digman MA, Gratton E. Raster image correlation spectroscopy in live cells. *Nat Protoc*. 2010;5(10). doi:10.1038/nprot.2010.122.
74. Digman MA, Brown CM, Sengupta P, et al. Measuring fast dynamics in solutions and cells with a laser scanning microscope. *Biophys J*. 2005;89(2):1317-1327.

doi:10.1529/biophysj.105.062836.

75. Digman MA, Wiseman PW, Horwitz AR, Gratton E. Detecting Protein Complexes in Living Cells from Laser Scanning Confocal Image Sequences by the Cross Correlation Raster Image Spectroscopy Method. *Biophys J*. 2009;96:707-716. doi:10.1016/j.bpj.2008.09.051.
76. Gratton E. *Introduction to Advanced FCS*. Irvine; 206AD. http://www.lfd.uci.edu/workshop/2006/files/LFDWorkshop2006-Lecture01.pdf.
77. Meng F, Ma H, And FM, Hui Ma* †. A Comparison between Photon Counting Histogram and Fluorescence Intensity Distribution Analysis. *J Phys Chem B*. 2006;110:25716-25720. http://pubs.acs.org.eres.library.manoa.hawaii.edu/doi/abs/10.1021/jp063845r. Accessed March 4, 2017.
78. Kask P, Palo K, Ullmann D, Gall K. Fluorescence-intensity distribution analysis and its application in biomolecular detection technology. *Proc Natl Acad Sci U S A*. 1999;96(24):13756-13761. doi:10.1073/PNAS.96.24.13756.
79. Digman MA, Dalal R, Horwitz AF, Gratton E. Mapping the Number of Molecules and Brightness in the Laser Scanning Microscope. *Biophys J*. 2008;94(6):2320-2332. doi:10.1529/biophysj.107.114645.
80. Digman MA, Wiseman PW, Choi C, Horwitz AR, Gratton E. Stoichiometry of molecular complexes at adhesions in living cells. *Proc Natl Acad Sci U S A*. 2009;106(7):2170-2175. doi:10.1073/pnas.0806036106.
81. Unruh JR, Gratton E. Analysis of molecular concentration and brightness from fluorescence fluctuation data with an electron multiplied CCD camera. *Biophys J*. 2008;95(11):5385-5398. doi:10.1529/biophysj.108.130310.
82. Redford GI, Clegg RM. Polar Plot Representation for Frequency-Domain Analysis of Fluorescence Lifetimes. *J Fluoresc*. 2005;15(5):8015-8815. doi:10.1007/s10895-005-2990-8.
83. Vetromile CM, Jameson DM. Frequency Domain Fluorometry: Theory and Application. In: Engelborghs Y, Visser AJWG, eds. *Fluorescence Spectroscopy and Microscopy: Methods and Protocols*. ; 2014:77-95. doi:10.1007/978-1-62703-649-8_5.
84. Weber G. Resolution of the fluorescence lifetimes in a heterogeneous system by phase and

modulation measurements. *J Phys Chem*. 1981;85(8):949-953. doi:10.1021/j150608a006.

85. Gratton E, Jameson DM, Hall RD. Multifrequency Phase and Modulation Fluorometry. *Ann Rev Biophys Bioeng*. 1984;13:105-124. http://www.annualreviews.org.eres.library.manoa.hawaii.edu/doi/pdf/10.1146/annurev.bb.13.060184.000541. Accessed March 2, 2017.
86. Spencer RD, Weber G. Measurements of subnanosecond fluorescence lifetimes with a cross-correlation phase fluorometer. *Ann N Y Acad Sci*. 1969;158(1 Electronic As):361-376. doi:10.1111/j.1749-6632.1969.tb56231.x.
87. Noomnarm U, Clegg RM. Fluorescence lifetimes: fundamentals and interpretations. 2009. doi:10.1007/s11120-009-9457-8.
88. Jameson DM, Vetromile CM, James NG, Schuck P. Investigations of protein-protein interactions using time-resolved fluorescence and phasors. *Methods*. 2013;59:278-286. doi:10.1016/j.ymeth.2013.01.004.
89. James NG, Ross JA, Štefl M, Jameson DM. Applications of Phasor Plots to in Vitro Protein Studies. *Anal Biochem*. 2011;410. doi:10.1016/j.ab.2010.11.011.
90. Förster T. Energy migration and fluorescence. *J Biomed Opt*. 2012;17(1):11002. doi:10.1117/1.JBO.17.1.011002.
91. Periasamy A, Vogel SS, Clegg RM. FRET 65: A Celebration of Förster. *J Biomed Opt*. 2012;17(1). doi:10.1117/1.JBO.17.1.011001.
92. Ross JA, Gilmore MA, Williams D, Aoki KR, Steward LE, Jameson DM. Characterization of Forster resonance energy transfer in a botulinum neurotoxin protease assay. *Anal Biochem*. 2011;413:43-49. doi:10.1016/j.ab.2011.01.045.
93. Akrap N, Seidel T, George Barisas B. Förster distances for FRET between mCherry and other Visible Fluorescent Proteins. *Anal Biochem*. 2010;402:105-106. doi:10.1016/j.ab.2010.03.026.
94. Chen Y, Müller JD, So PTC, et al. The Photon Counting Histogram in Fluorescence Fluctuation Spectroscopy. *Biophys J*. 1999;77(1):553-567. doi:10.1016/S0006-3495(99)76912-2.
95. Digman MA, Gratton E. Scanning Image Correlation Spectroscopy. *Bioessays*. 2013;34(5):377-385. doi:10.1002/bies.201100118.

96. Shehata M, Matsumura H, Okubo-Suzuki R, Ohkawa N, Inokuchi K. Cellular/Molecular Neuronal Stimulation Induces Autophagy in Hippocampal Neurons That Is Involved in AMPA Receptor Degradation after Chemical Long-Term Depression. doi:10.1523/JNEUROSCI.4533-11.2012.
97. Macıas W, Carlson R, Rajadhyaksha A, Barczak A, Konradi C. Potassium chloride depolarization mediates CREB phosphorylation in striatal neurons in an NMDA receptor-dependent manner. https://www.ncbi.nlm.nih.gov/pmc/articles/PMC4203340/pdf/nihms-197429.pdf. Accessed March 16, 2017.
98. Digman MA, Stakic M, Gratton E. Raster Image Correlation Spectroscopy and Number and Brightness Analysis. *Methods Enzymol*. 2013;518:121-144. doi:10.1016/B978-0-12-388422-0.00006-6.
99. Lu W, Ziff EB. PICK1 Interacts with ABP/GRIP to Regulate AMPA Receptor Trafficking. *Neuron*. 2005;47:407-421. doi:10.1016/j.neuron.2005.07.006.
100. Hanley JG. Actin-dependent mechanisms in AMPA receptor trafficking. *Front Cell Neurosci*. 2014;8:381. doi:10.3389/fncel.2014.00381.
101. James NG, Digman MA, Ross JA, et al. A mutation associated with centronuclear myopathy enhances the size and stability of dynamin 2 complexes in cells. *Biochim Biophys Acta - Gen Subj*. 2014;1840(1):315-321. doi:10.1016/j.bbagen.2013.09.001.
102. Dasilva LLP, Wall MJ, De Almeida LP, et al. Activity-Regulated Cytoskeleton-Associated Protein Controls AMPAR Endocytosis through a Direct Interaction with Clathrin-Adaptor Protein 2 1,2,3. *eNeuro*. 2016;3(3):1-22. doi:10.1523/ENEURO.0144-15.2016.
103. Zhang W, Wu J, Ward MD, et al. Structural Basis of Arc Binding to Synaptic Proteins: Implications for Cognitive Disease. *Neuron*. 2015;86(2):490-500. doi:10.1016/j.neuron.2015.03.030.
104. Huber KM, Roder JC, Bear MF. Chemical induction of mGluR5- and protein synthesis--dependent long-term depression in hippocampal area CA1. *J Neurophysiol*. 2001;86(1):321-325. http://www.ncbi.nlm.nih.gov/pubmed/11431513. Accessed March 18, 2017.